TropFlux wind stresses over the tropical oceans: evaluation and comparison with other products

**B. Praveen Kumar · J. Vialard · M. Lengaigne ·
V. S. N. Murty · M. J. McPhaden · M. F. Cronin ·
F. Pinsard · K. Gopala Reddy**

Abstract In this paper, we present TropFlux wind stresses and evaluate them against observations along with other widely used daily air-sea momentum flux products (NCEP, NCEP2, ERA-I and QuikSCAT). TropFlux wind stresses are computed from the COARE v3.0 algorithm, using bias and amplitude corrected ERA-I input data and an additional climatological gustiness correction. The wind stress products are evaluated against dependent data from the TAO/TRITON, PIRATA and RAMA arrays and independent data from the OceanSITES mooring networks. Wind stress products are more consistent amongst each other than surface heat fluxes, suggesting that 10 m-winds are better constrained than near-surface thermodynamical parameters (2 m-humidity and temperature) and surface downward radiative fluxes. QuikSCAT overestimates wind stresses away from the equator, while NCEP and NCEP2 underestimate wind stresses, especially in the equatorial Pacific. QuikSCAT wind stress quality is strongly affected by rain under the Inter Tropical Convergence Zones. ERA-I and TropFlux display the best agreement with in situ data, with correlations >0.93 and rms-differences <0.012 Nm^{-2}. TropFlux wind stresses exhibit a small, but consistent improvement (at all timescales and most locations) over ERA-I, with an overall 17 % reduction in root mean square error. ERA-I and TropFlux agree best with long-term mean zonal wind stress observations at equatorial latitudes. All products tend to underestimate the zonal wind stress seasonal cycle by ∼20 % in the western and central equatorial Pacific. TropFlux and ERA-I equatorial zonal wind stresses have clearly the best phase agreement with mooring data at intraseasonal and interannual timescales (correlation of ∼0.9 versus ∼0.8 at best for any other product), with TropFlux correcting the ∼13 % underestimation of ERA-I variance at both timescales. For example, TropFlux was the best at reproducing westerly wind bursts that played a key role in the 1997–1998 El Niño onset. Hence, we recommend the use of TropFlux for studies of equatorial ocean dynamics.

Keywords TropFlux · Tropics · Air-sea momentum fluxes · Wind stress products validation

B. Praveen Kumar (✉) · M. Lengaigne
Physical Oceanography Division,
National Institute of Oceanography, Council of Scientific
and Industrial Research, Dona Paula, Goa 403004, India
e-mail: pkb_ocean@yahoo.co.in; bpraveen@nio.org

J. Vialard · M. Lengaigne · F. Pinsard
Laboratoire d'Océanographie Expérimentation et Approches
Numériques, CNRS, UPMC, IRD, Paris, France

V. S. N. Murty
National Institute of Oceanography, Regional Centre,
Council of Scientific and Industrial Research,
Vishakhapatnam, India

M. J. McPhaden · M. F. Cronin
NOAA/Pacific Marine Environmental Laboratory,
Seattle, WA, USA

K. Gopala Reddy
Department of Meteorology and Oceanography,
Centre for Bay of Bengal Studies,
Andhra University, Vishakhapatnam, India

1 Introduction

The tropics are home to many climatically relevant phenomena. The two most spectacular examples of such globally relevant modes of climate variability are the El Niño Southern Oscillation (ENSO) and Madden-Julian Oscillation (MJO). ENSO is the strongest mode of

interannual climate variability on the planet (e.g., McPhaden 2004; McPhaden et al. 2006). Although it largely arises from positive air-sea feedbacks in the tropical Pacific, it has consequences that are felt around the world. The MJO is the dominant mode of intraseasonal variability, with worldwide teleconnections (e.g., Zhang 2005) including impacts on weather over the North Atlantic (Cassou 2008). There is also well-known ocean–atmosphere interannual variability in the Indian Ocean (the Indian Ocean Dipole or IOD, e.g., Saji et al. 1999; Webster et al. 1999) and in the tropical Atlantic (the Atlantic Meridional Mode, e.g., Xie and Carton 2004).

For most of the aforementioned climate phenomena, air-sea interactions play an essential role. For instance, ENSO and IOD events grow as a result of the so-called Bjerknes feedback (e.g., Bjerknes 1966; Wang and Picaut 2004; Annamalai et al. 2003). The Bjerknes feedback involves the following loop: surface momentum flux anomalies induce changes in ocean circulation that lead to the growth of Sea Surface Temperature (SST) anomalies, which in turn reinforce the original momentum flux anomalies. Surface momentum fluxes (i.e. wind stresses, generally expressed in units of Nm^{-2}) are hence an essential measure of the air-sea coupling in the Bjerknes feedback. While ocean–atmosphere coupling is associated to a larger extent with surface heat fluxes rather than to surface wind stresses for MJO events (e.g., Duvel and Vialard 2007; Jayakumar et al. 2011; Drushka et al. 2011; Vialard et al. 2012), equatorial wind stress perturbations associated with the MJO drive strong basin-wide dynamical response, both in the Indian Ocean (e.g., Han et al. 2011; Vialard et al. 2009; Nagura and McPhaden 2012) and the Pacific Ocean (e.g., Zhang and McPhaden 2006; Lengaigne et al. 2002). Westerly wind bursts in the western equatorial Pacific induce westward currents in the central Pacific that play a key role in the westward migration of the warm pool associated with the onset of El- Niño events (Lengaigne et al. 2004). At decadal timescales, there is also evidence of clear, Indo-Pacific wide sea level variations forced by wind stress variations (e.g., Lee and McPhaden 2008; Han et al. 2010; Nidheesh et al. 2012).

Wind stress is not only important in air-sea interactions and forced oceanic variability, as mentioned above, but also plays an important role in the tropical mean state. The pressure gradient associated with climatological east–west tilt of the thermocline in the tropical Pacific and Atlantic oceans is to first order in balance with zonal wind stress (e.g., McCreary 1981a, b). The strong Wyrtki jets that develop in spring and fall in the equatorial Indian Ocean result from the semi-annual relaxation of the weak westerlies that otherwise prevail (e.g., Schott and McCreary 2001; Nagura and McPhaden. 2010a). Away from the equator, wind stress curl also plays a prominent role in setting

equatorial current systems like the South Equatorial Current or North Equatorial Counter-Current in the Atlantic and Pacific oceans (Rodrigues et al. 2007; Kessler et al. 2003).

Accurate knowledge of air-sea momentum fluxes is thus important to study the tropical mean state and variability from intraseasonal to decadal time-scales. Momentum fluxes are usually calculated from wind speed using the empirical formulae $\tau = \rho\, C_d\, w^2$ where τ is the wind stress magnitude, ρ is surface air density, C_d the drag coefficient, and w the wind speed relative to the ocean surface (often assumed to be stationary). The drag coefficient is in principle a non-linear function of the wind speed, atmospheric stability and sea state. There is a wide choice of different methods available in literature for drag coefficient calculation (Smith 1988; Large and Pond 1981; Hellerman and Rosenstein 1983; Fairall et al. 1996, 2003). Assessing the relative merits of different drag coefficient estimation methods is not the aim of this study, and has been discussed elsewhere (Bruke et al. 2003; Kochanski et al. 2006). In this paper, we have selected the COARE v3.0 algorithm because it takes atmospheric stability into account, has been developed purposely for tropical regions, and provides an estimated accuracy of 5 % (for wind speed below $10~ms^{-1}$) or 10 % (for wind speed from 10 to $20~ms^{-1}$) (Fairall et al. 2003).

While there are uncertainties in drag formulae, another source of uncertainty in surface momentum flux estimates is wind speed itself. Historically, ship-based observations provide the major source of wind data over the global oceans (e.g., Bunker 1976; Hellerman and Rosenstein 1983; da Silva et al. 1994; Josey et al. 2002). One major drawback of observation based momentum flux datasets is the poor spatial and temporal coverage of in situ measurements. In situ observation based momentum fluxes are largely limited to frequent shipping lines in the northern hemisphere (Risien and Chelton 2008) and do not span more than 1 month for each cruise. In situ observation based momentum fluxes thus generally do not exceed 1-month temporal resolution. The increase in ship size and related higher anemometer heights above the ocean surface has also led to a bias towards increased wind speeds (Tokinaga and Xie 2011).

Of late, two interesting alternatives provide higher resolution wind speed datasets over the tropical oceans: satellite scatterometry and re-analyses. Satellite scatterometers are designed to measure surface wind speed and direction by electromagnetic radar backscatter from the rough ocean surface at different angles. One of the most successful and widely used scatterometer missions is QuikSCAT, starting in July 1999 and ending in October 2009, whose sun-synchronous orbit allowed it to sample 90 % of the global ocean daily (Schlax et al. 2001). One major drawback of these efforts using satellite data

products is their limited life span since most of the satellite missions last about 10 years or less. While the focus of this paper is on timely wind stresses products, we include QuikSCAT in our wind stress evaluations because it is a widely used product that was available until recently.

Re-analyses also provide an interesting alternative for estimating wind variations at high temporal resolution. Re-analyses are generated at operational weather centers using an up-to-date version of numerical weather forecasting model and data assimilation system to retrospectively re-process past atmospheric observations over a long period. The advantage of re-analyses is that they take advantage of any relevant information to estimate wind speed (e.g., pressure, through the geostrophic relation) and use numerical models to spatially and temporally interpolate sparse data. Recent timely re-analyses include the National Centre for Environmental Prediction (NCEP reanalysis, 1948–present, Kalnay et al. 1996), the Department of Energy (DOE) or NCEP2 re-analysis (1979–present, Kanamitsu et al. 2002), and the new European Centre for Medium Range Weather Forecast interim re-analysis (ERA-I, 1979–present, Dee et al. 2011). Note also the recent effort by the OAFlux project to provide a synthesis from the various existing re-analyses and surface observations (Yu et al. 2007). While this project provides good quality surface flux and wind data, it does not, however, yet provide surface momentum flux estimates.

Several past studies have used in situ data to evaluate wind stress products or have compared existing products. Rienecker et al. (1996), Pegion et al. (2000) and Meissner et al. (2001) compare several satellite, in situ and re-analysis based wind products. Bentamy et al. (1996) and Chelton and Freilich (2005) evaluate scatterometer wind stress products against mooring data. Josey et al. (2002) evaluate an in situ data based wind stress climatology against climatologies derived from other in situ datasets, re-analyses and operational wind products. Hackert et al. (2001) compare winds products during the 1997–1998 El Niño event through the use of an ocean general circulation model. But to our knowledge, there is no published extensive intercomparison and evaluation of recent, timely wind stress estimates from re-analyses (NCEP, NCEP2, ERA-I) against available in situ observations.

In a companion paper (Praveen Kumar et al. 2012), we introduced a new, timely air-sea heat flux product with daily resolution for the tropical region (30°N-30°S)—Trop-Flux—and evaluated it, along with other products (NCEP, NCEP2, ERA-I, OAFlux), against available observations from the global tropical moored buoy array (McPhaden et al. 1998; Bourlès et al. 2008; McPhaden et al. 2010) and OceanSITES (http://www.OceanSITES.org) data. In the present paper, we build on the methodology presented in Praveen Kumar et al. (2012) to estimate TropFlux wind-

stresses, and compare them with other products (NCEP, NCEP2, ERA-I and QuikSCAT wind stresses) and estimates from moored buoys. The rest of the paper is organized as follows. Section 2 describes the various datasets used in this study. In Sect. 3, we describe the TropFlux wind stress computation methodology, and evaluate TropFlux against ERA-I, from which it is derived. A detailed evaluation and validation of TropFlux, NCEP, NCEP2, ERA-I and QuikSCAT wind stress products are provided in Sect. 4, including a discussion of their differences at various time-scales (long term-bias, interannual, seasonal and intraseasonal variability), with a focus on equatorial dynamics. We summarize and discuss the main results in Sect. 5.

2 Datasets

In this section we describe the various wind stress products evaluated in this paper, the (dependent) global tropical moored buoy array evaluation data, and the independent data from OceanSITES project. Praveen Kumar et al. (2012) provide a detailed description of these datasets, and we will hence present them in a more concise way below.

2.1 Gridded data products

We used three re-analyses (NCEP, NCEP2 and ERA-I) and one satellite based gridded wind stress product (Quik-SCAT) in this study. All four daily products were re-gridded to a common 1° × 1° grid.

NCEP re-analysis extends from 1948 to present, with an original ∼1.9° resolution (Kalnay et al. 1996). NCEP2 re-analysis is an alternative version of NCEP reanalysis, which addresses some of the known problems of NCEP re-analysis (Kanamitsu et al. 2002). The main modifications likely to affect wind over the oceans in NCEP2 are a new shortwave radiation and cloud scheme. NCEP2 is available from 1979 to present. We use daily average wind stresses from NCEP and NCEP2, obtained as the mean of four 6 h-averages obtained from the first 6 h of the 00, 06, 12, and 18UTC forecasts. The ERA-I re-analysis (Dee et al. 2011), available from 1979 to present, uses an advanced 4-D Var assimilation approach, and provides data at a higher 0.75° spatial resolution. ERA-I 10 m winds, 2 m air temperature and humidity are obtained as the mean of 4 analyzed fields at 00, 06, 12 and 18 UTC. Wind-stress from ERA-I is computed as the average of the two 12-h forecasts starting at 00 and 12UTC. The boundary layer scheme used in the ERA-I re-analysis has a formulation in essence very similar to the COARE v3.0 algorithm (A. Beljaars, personal communication, 2012).

CERSAT (Centre ERS d'Archivage et de Traitement) provides gridded fields of wind parameters retrieved from

the NASA (National Aeronautics and Space Administration) Scatterometer on board QuikSCAT at $0.5° \times 0.5°$ resolution over the global oceans (80°S–80°N) from July 1999 to November 2009 which was the end of the satellite mission (Bentamy et al. 2002). Daily average synoptic fields are obtained from discrete observations from a statistical interpolation with an objective method. QuikSCAT uses Smith (1988) drag coefficient scheme for stress computation, but only takes wind speed variation into account (surface air temperature and humidity variations are neglected). Several studies (e.g., Milliff et al. 2004; Gille 2005; Bentamy et al. 2012) have already underlined that wind speed (and stress) retrieval is very difficult in rainy conditions because of the backscatter of raindrops in the atmospheric column above the surface. The CERSAT version of QuikSCAT data uses the Impact based Multidimensional Histogram method (see Huddleston and Stiles. 2000 for details) for rain flagging. Bentamy et al. (2012) recently demonstrated that their estimation of wind speed could be significantly improved by applying a stricter flagging of rainy situations, but this improved estimate is not available yet. As discussed in the introduction, the wind stress is normally computed as a function of the wind speed relative to the sea surface (i.e. from vector winds minus vector currents). The advantage of satellite scatterometers is that they directly provide an estimate of stress at the ocean surface, and hence naturally account for the effect of currents on wind stress (Bentamy et al. 2003; Chelton and Freilich. 2005).

2.2 Global tropical moored buoy array

The Global Tropical Moored Buoy Array (McPhaden et al. 2010, see Figure 1 for mooring locations) is a multinational effort providing surface meteorological and subsurface oceanic near-real time data for research and applications. It has three components, namely TAO/TRITON in the tropical Pacific (McPhaden et al. 1998), PIRATA in the tropical Atlantic (Bourlès et al. 2008) and RAMA in the tropical Indian Ocean (McPhaden et al. 2009). Hereafter data from the tropical moored array will be referred to as TPR data (for TAO/TRITON-PIRATA-RAMA).

Moorings from the TPR network measure wind speed at about 4 m-height and air temperature and humidity at 3 m-height. Wind stresses are computed from the telemetered daily average zonal and meridional winds, using the COARE v3.0 algorithm, as described in Cronin et al. (2006), and are available from the TAO Project OceanSITES page (http://www.pmel.noaa.gov/tao/OceanSITES/index.html). A diurnal gustiness factor, computed at each site from higher frequency wind data when available, is used to account for wind variations shorter than 1 day,

similar to the approach described in Cronin et al. (2006). The TPR wind stresses are computed both from absolute wind velocity and relative wind velocities when surface layer (typically at 10 m depth) currents are available from the moorings. Since surface layer currents are less frequently available than other meteorological parameters, the TPR relative stress database is not as complete as the absolute one (only 1/5th of data compared to the absolute stress database). As demonstrated in the TPR fluxes documentation (see http://www.pmel.noaa.gov/tao/oceansites/flux/documentation.html), the TPR absolute and relative wind stresses are very similar (0.99 correlation, less than 0.006 Nm^{-2} rmd-difference in wind stress norm over the entire dataset). Hence, unless otherwise specified, we use the larger absolute wind stress database in the rest of the paper.

TPR data undergo stringent quality control procedures to ensure high accuracy standards (Freitag et al. 1999, 2001; Medavaya et al. 2002; Payne et al. 2002; Lake et al. 2003). We only use daily wind stress data with quality flags one and two (highest or default quality) when evaluating other products. Figure 1a shows the total number of valid data for the entire QuikSCAT record (20 July 1999 to 13 October 2009), the shortest record among the wind stress products we analyze. TAO/TRITON is the first mooring array that was initiated (Fig. 1b), and most moorings over the Pacific Ocean have between 5 and 10 years of daily data over the QuikSCAT period. The PIRATA array was the next one to be deployed (Fig. 1b), and most moorings provide 2–7 years of data. The shortest records are in the Indian Ocean (Fig. 1b), with no mooring exceeding a total of 3 years of valid data. The number of high quality daily observations from the TPR array is quite stable (around 50) since 1999.

The statistics in the paper are shown for comparison of 5-day averaged TPR and re-analysis data valid at the same time. This 5-day averaging was introduced to avoid giving too much weight to very high frequency wind variations. Note, however, that qualitatively very similar conclusions are obtained when computing statistics from daily data. Most statistics presented in this paper were computed over a common period of 1 August 1999–31 July 2009, which includes the entire QuikSCAT period, except for a few months near the beginning and end of the QuikSCAT record so that we retain exactly 11 full seasonal cycles. From now on, the "QuikSCAT period" refers to this 11-years long evaluation period.

The overall statistics mentioned above do not distinguish the ability of various datasets to reproduce observed variability at different time scales (intraseasonal, seasonal, interannual variability etc.). We thus also provide statistics for each of these timescales. The TPR intraseasonal variability is defined here as 10–90 day filtered data using a

Fig. 1 **a** Total length of valid (quality flag 1 or 2) wind stress estimates, in years, over the QuikSCAT period (1st August 1999 to 31st July 2009) at TPR (TAO-TRITON/PIRATA/ RAMA) sites. Only mooring locations with more than 180 days of high quality data are shown here. *Black asterisks* indicate locations of independent OceanSITES validations sites. **b** Total number of high quality wind stress estimates available from the TPR array per day. The *black*, *red* and *blue lines* in *bottom panel* represent the period over which data are available from TAO/TRITON, PIRATA and RAMA respectively
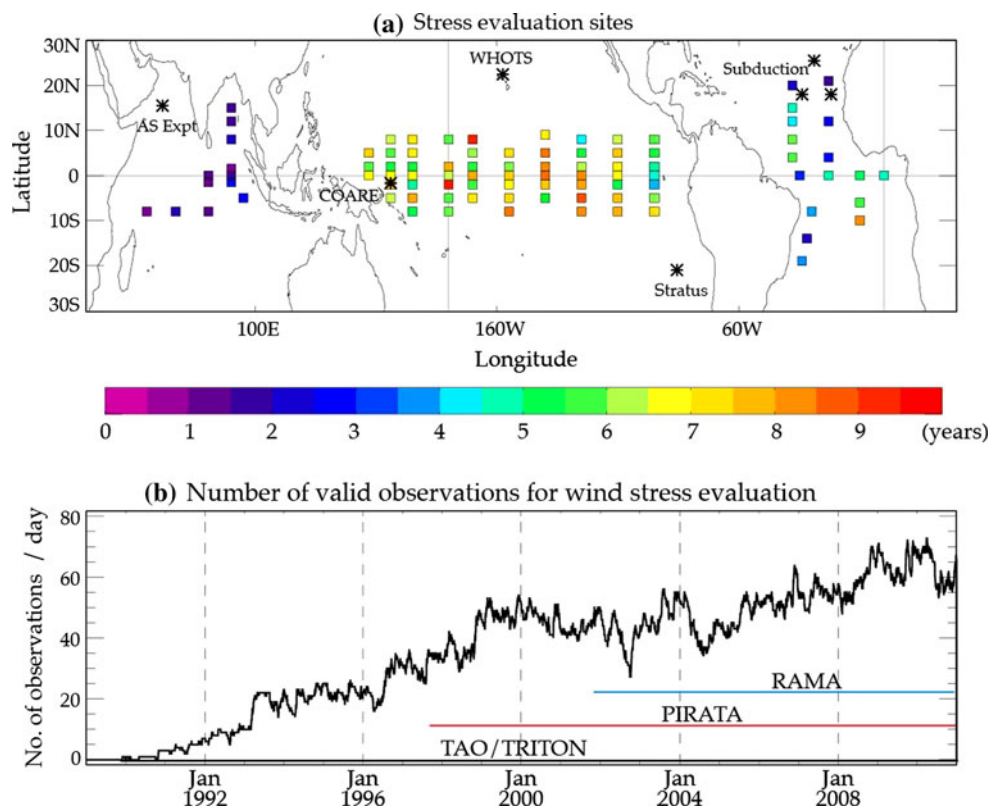
101-point digital filter. This 10–90 day window was chosen because it includes both MJO timescales (most energetic between ∼20 and 80 days, e.g., Wheeler and Hendon 2004) and westerly wind bursts, which play an important role in El Niño onset, and have typical durations of 10–20 days (e.g., Lengaigne et al. 2004). This procedure causes ∼50 days of data to be lost on both ends of any segment of uninterrupted data. We computed the TPR mooring seasonal cycle by fitting the first 3 harmonics of the annual cycle (365, 182.5 and 121.7 days) to any mooring with more than 5 years of data. The interannual anomalies are defined as 90-day low passed filtered differences between TPR original data and the fitted seasonal cycle (data are also lost on both sides of any segment of data due to filtering). We provide statistics for intraseasonal/seasonal/interannual variability only for those moorings with more than 1/4/7 years of valid data. This means that, while we can evaluate intraseasonal variations in the three tropical oceans, we can only evaluate the mean seasonal cycle in the Atlantic and Pacific, and interannual variability in the Pacific.

While they provide valuable data against which to compare re-analyses, TPR data do not provide a fully independent validation. The TPR data are assimilated in most of the re-analysis products. We will hence talk about "evaluation" when comparing various datasets to the dependent TPR data, and about "validation" when using the independent OceanSITES dataset discussed below.

2.3 Independent validation data sets

Since comparison with TPR observations provides only partially independent evaluation, we also use data from five mooring locations collected over the last two decades by Woods Hole Oceanographic Institution (WHOI). These datasets are withheld from operational data streams and hence provide a completely independent dataset for re-analyses validation purposes. The five moorings are from: Arabian Sea experiment (Arabian Sea Mixed Layer Dynamics Experiment; Weller et al. 1998), COARE experiment (Coupled Ocean–Atmosphere Response Experiment; Webster and Lukas 1992), WHOTS experiment (WHOI Hawaii Ocean Time series Station Experiment; Plueddemann et al. 2006; Whelan et al. 2007), Stratus experiment (Colbo and Weller 2007) and the Subduction experiment (Brink et al. 1995). These locations are shown as black asterisks in Fig. 1.

These moorings provide high quality, hourly meteorological and oceanographic data over periods ranging from a few months to a few years. We use these data to produce hourly time series of wind stresses using COARE v3.0 (Fairall et al. 1996, 2003) algorithm. We apply no gustiness correction other than the one built in the COARE v3.0 algorithm in this computation, and obtain daily wind stresses from the hourly values. Note that, we neglected surface currents (which are not always available) while computing wind stresses at these moorings.

3 The TropFlux wind stress product

In this section, we first present the methodology for computing TropFlux momentum fluxes. Since those rely heavily upon ERA-I data, we then present a comparison of TropFlux and ERA-I to TPR data, to investigate the added value of TropFlux.

3.1 Estimation method

The TropFlux project aims at producing high quality daily, timely heat and momentum fluxes over the tropical oceans. The companion paper by Praveen Kumar et al. (2012) describes the development of TropFlux heat fluxes and shows that, together with OAFlux heat fluxes (Yu et al. 2007), it compares best to TPR and OceanSITES data. In this section, we present the methodology of TropFlux wind stress computation, largely derived from Praveen Kumar et al. (2012). TropFlux wind stresses are available at $1° × 1°$, daily resolution within 30°S–30°N from 1979 to almost near real time from http://www.locean-ipsl.upmc.fr/tropflux or http://www.nio.org.

We use the strategy of Cronin et al. (2006) for computing wind stresses:

$$\tau = \rho_a C_d s^2 \qquad (1)$$

$$s = \left(w^2 + w_g^2\right)^{1/2} \qquad (2)$$

where τ is the estimated daily wind stress magnitude, ρ_a surface air density, C_d the drag coefficient computed by the COARE v3.0 algorithm (as a function of sea surface temperature, 2 m-air temperature and humidity, 10 m-wind), w the daily-average wind speed and w_g a climatological diurnal gustiness. The climatological gustiness w_g is calculated following Praveen Kumar et al. (2012) as a function of long term-mean SST, with the mean relation between gustiness and SST derived from the gustiness at each TPR site computed as in Cronin et al. (2006). Following the TPR methodology, the zonal and meridional components of momentum flux are obtained as:

$$\tau_x = \tau(u/s) \qquad (3)$$

$$\tau_y = \tau(v/s) \qquad (4)$$

where u and v are the 10 m-wind daily average zonal and meridional components.

The basic input variables necessary to compute wind stresses using this strategy are hence the 2 m-air temperature and humidity, 10 m-wind and SST. Detailed evaluation of these variables against TPR observations suggests that ERA-I performs better than other sources of data but with some caveats such as systematic biases and reduced variability (see Figure 3 of Praveen Kumar et al. 2012). We

hence use here the same bias and amplitude correction strategy as in Praveen Kumar et al. (2012). Briefly, all ERA-I variables are corrected from a spatially homogenous long-term bias estimated from TPR data, except temperature for which a spatially dependent bias is applied as a function of climatological air temperature. All variables are also multiplied by a constant coefficient fitted on TPR data. For wind speed, the correction is obtained as $w_c = [1.11w' + (w_m + 0.28)]$ with units in ms^{-1}, where w_m is the long term mean and w' is the anomaly with respect to long term mean. We use this corrected wind speed to compute s from Eq. 2, and then use this s in Eqs. (1), (3) and (4).

As indicated by Eqs. (1) or (2), we use absolute winds when computing surface wind stresses, and hence do not account for the effect of surface currents. There are two additional options to account for the effect of surface waves on the wind stress estimate in Fairall et al. (2003) but we did not use them in the current TropFlux wind stress estimates. We will discuss the effect of those approximations in the Sect. 5.

3.2 TropFlux versus ERA-I wind stresses

TropFlux momentum fluxes are largely derived from ERA-I basic variables. In this subsection, we compare TropFlux and ERA-I to TPR data in order to evaluate the added value of the TropFlux product. We show statistics for the wind stress modulus, but the same conclusions can be drawn for the zonal and meridional components (not shown).

TropFlux differs from ERA-I momentum fluxes in the following ways:

1. ERA-I momentum fluxes are retrieved from forecast average wind-stress whereas TropFlux stresses are computed from the analyzed winds (and 2 m temperature and humidity) using a bulk formula. The boundary layer scheme used in ERA-I has a formulation in essence very similar to the COARE v3.0 algorithm (A. Beljaars, personal communication, 2012), so that this part of the difference should be dominated by differences in analyzed/forecast wind speed, more than the C_d formulation in Eq. (1).
2. Analyzed ERA-I variables are bias and amplitude corrected before fluxes are computed.
3. We apply a gustiness correction to account for unresolved subdiurnal wind variations.

In order to evaluate separately the influence of 1–3, Fig. 2 shows TPR evaluation statistics for the extracted ERA-I wind stresses (ERA-I), for wind stresses computed from the analyzed winds (ANA), from the analyzed winds with amplitude and bias correction (COR), from the analyzed winds with gustiness applied (GUST) and for TropFlux (see figure caption for details).
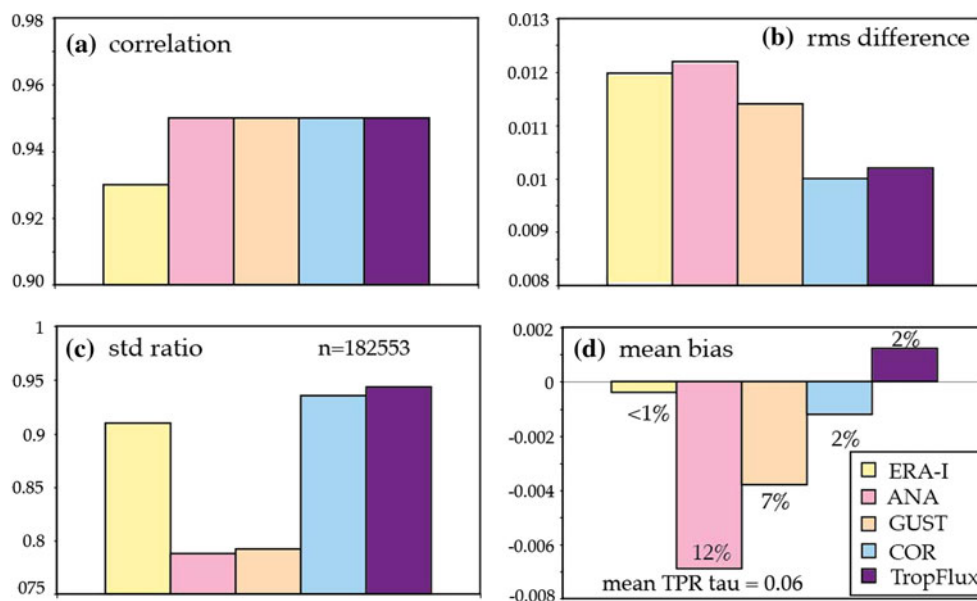
Fig. 2 *Bar diagrams* showing evaluation of 5-day average wind stress magnitude from different products to those computed from TPR (TAO-PIRATA-RAMA) moored buoy arrays. Statistics are computed at each site with more than 180 days of high quality data over QuikSCAT period and then averaged over the whole TPR array. Statistics from ERA-I stresses are shown in *yellow*. The *other colors* indicate the various steps in the TropFlux wind stresses computation: (see *text* for details). The stresses recomputed from analyzed ERA-I parameters (ANA) are shown in *pink*. Stresses recomputed with a gustiness correction (GUST) are shown in salmon. Stresses recomputed with a bias and amplitude correction (COR) are shown in *light blue*. TropFlux is shown in *purple*. The *percentages* in **d** correspond to percentage of deviation from the mean TPR value (0.06 Nm^{-2}). These statistics are computed against 182,553 high quality daily TPR observations

ERA-I wind stresses display very good phase agreement with TPR data (0.93 correlation, Fig. 2a) and negligible mean bias (Fig. 2d) but underestimate variability by $\sim$10 % (Fig. 2c). Re-computing wind stresses from the analysis rather than the forecasts slightly improves the phase agreement, but further diminishes the amplitude of wind stress variability, and results in a negative wind stress bias. Applying the gustiness correction reduces the mean bias, down to $\sim$7 % of the mean TPR value. Applying the wind correction reduces both the bias and improves the variability amplitude. Applying both the gustiness and wind correction together results in both a weak positive bias and amplitude of variability close to TPR data. Note that applying the gustiness does not clearly improve TropFlux stresses compared to COR. However, the same approach resulted in a notable improvement in the mean net heat flux bias values in Praveen Kumar et al. (2012). Hence for consistency, we keep the same approach for the wind stress computation here.

While TropFlux is marginally better than ERA-I in terms of its correlation and amplitude ratio to TPR stresses, its rms-error is 17 % smaller than that of ERA-I (Fig. 2b). While Fig. 2 provides an assessment of the overall improvement brought by TropFlux over the entire TPR array, Fig. 3 provides a systematic comparison of TropFlux and ERA-I evaluation statistics at each TPR mooring (and at each independent OceanSITES mooring). TropFlux corrections have a positive impact on the correlation and rms-error to mooring data at almost all sites (Fig. 3a and d). The

amplitude of the TropFlux wind stress variability is closer to mooring data at 61 sites out of 90 (Fig. 3c). The mean bias is reduced at 47 sites out of 90 (Fig. 3d), with TropFlux having a tendency to increase the bias in western Pacific.

The TropFlux approach is hence successful in adding value to ERA-I wind stresses. The improvement of TropFlux wind-stresses against ERA-I is however not as significant as the improvement we obtained on net heat fluxes (Praveen Kumar et al. 2012) mainly because ERA-I wind stresses were already very good, especially in terms of phase agreement and mean bias.

4 Evaluation of the stress products

In this section, we evaluate NCEP, NCEP2, ERA-I, TropFlux and QuikSCAT wind stresses from various sources against TPR mooring buoy observations. We then provide a completely independent validation against observations from five OceanSITES mooring locations. We discuss differences in climatological wind stress, before focusing on a dynamically important region: the equatorial band.

4.1 Evaluation against TPR data

Figure 4 shows overall statistics for the comparison of various products against TPR wind stress data. These statistics are evaluated over 1 August 1999–31 July 2009, the

Fig. 3 *Scatterplot* of evaluation statistics (over the QuikSCAT period) of TropFlux (*y*-axis) against ERA-I (*x*-axis) to TPR (*black diamonds* show statistics at each site) and OceanSITES (*red circles* show statistics at each site) mooring data. The **a** shows correlation, **b** shows mean bias at each mooring site, **c** shows the standard deviation ratio and **d** the root mean square difference. The *grey shading* on the *plot* delineates the sites where TropFlux is improved with respect to ERA-I for a given statistic
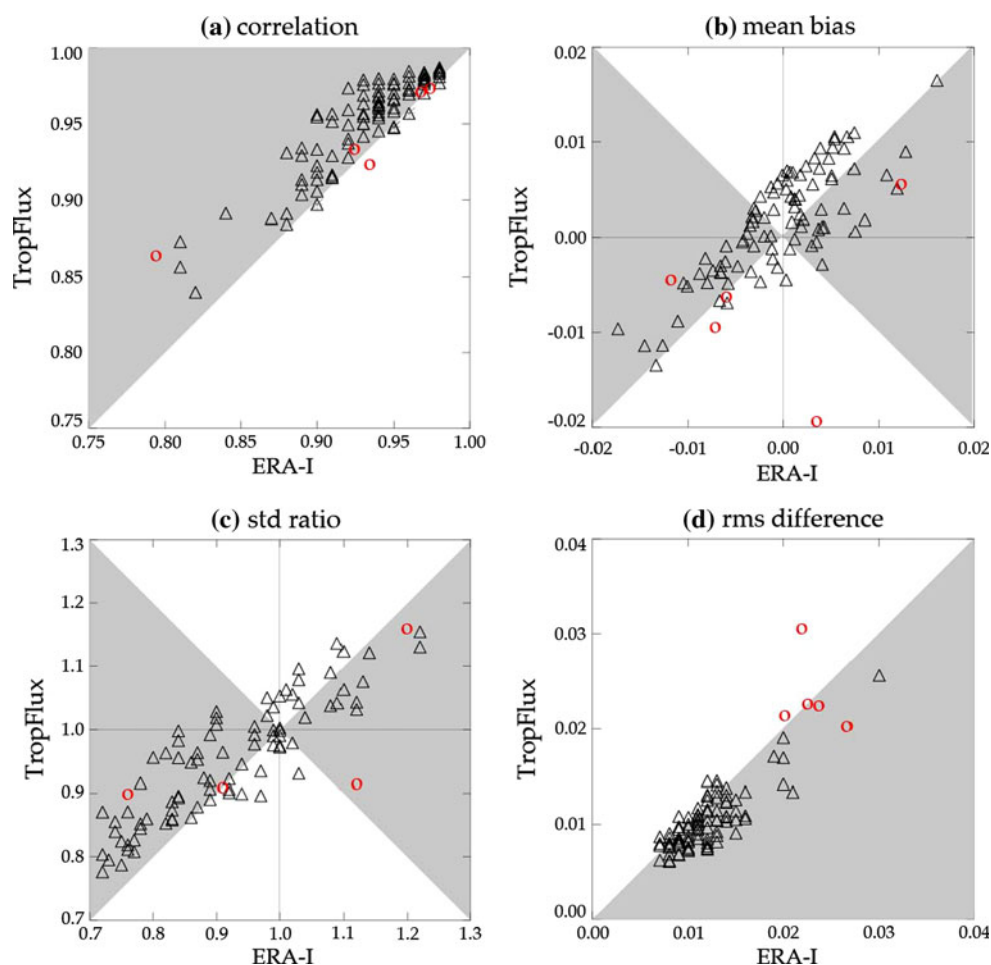
longest common period with QuikSCAT. We show statistics for the wind stress magnitude, but statistics for zonal and meridional components display very similar features (the only exception is that QuikSCAT meridional wind stress component is generally more accurate than the zonal component). NCEP and QuikSCAT display the largest bias in terms of mean state (Fig. 4b) and std ratio (Fig. 4c) with opposite tendencies. NCEP underestimates the amplitude of TPR wind stress variability by 24 % while QuikSCAT overestimates it by 17 %. NCEP also tends to display a strong negative mean bias (19 % of the mean TPR value), while QuikSCAT displays a strong positive bias (28 % of the mean TPR value). These results are generally consistent with previous studies discussing NCEP (Josey et al. 2002; Meissner et al. 2001) and QuikSCAT accuracy (e.g., Satheesan et al. 2007; Jiang et al. 2005). In contrast, NCEP2 and ERA-I capture the amplitude of wind stress variability better along with its mean value. ERA-I however displays a far better phase agreement (0.93 correlation) than NCEP and NCEP2 (0.83).

Figure 4 hence illustrates that ERA-I data is overall the best re-analysis product. Despite this enviable property,

ERA-I still underestimates the variability by about 9 % (Fig. 4c). This supports the choices we made in Praveen Kumar et al. (2012): 1) select ERA-I as TropFlux input data; 2) but apply a bias and amplitude correction. The TropFlux dataset captures the variability remarkably well with the highest correlation/lowest-rms difference to TPR data (0.95/0.01 Nm^{-2}). It has a weak mean bias ($\sim$2 % of the mean TPR data), and captures the amplitude fairly well ($\sim$5 % underestimation of the variability).

Statistics in Fig. 4 provide an overall evaluation of TropFlux for all TPR sites taken collectively. Figure 5 allows a more regional view. The color of the marker gives the correlation and rms-difference of TropFlux to TPR data. Square markers indicate locations where TropFlux outperforms all other products (i.e. highest correlation for upper panels and lowest rms-difference for lower panels). TropFlux displays the highest correlation and the lowest rms-difference to TPR data at most sites, both for zonal and meridional wind stresses. This analysis suggests that TropFlux not only displays the best overall agreement with TPR data, but also generally agrees best at individual locations.

Fig. 4 *Bar diagrams* showing evaluation of 5-day average wind stress magnitude from different products to those computed from TPR (TAO-PIRATA-RAMA) moored buoy arrays. Statistics are computed at each site with more than 180 days of high quality data over QuikSCAT period and then averaged over the whole TPR array. NCEP is shown in *blue*, NCEP2 in *red*, ERA-I in *yellow*, TropFlux in *purple*, and QuikSCAT in *light purple*. The *percentages* in **d** correspond to percent of deviation from the mean TPR value (0.06 Nm^{-2}). These statistics are computed against 182,553 high quality daily TPR observations
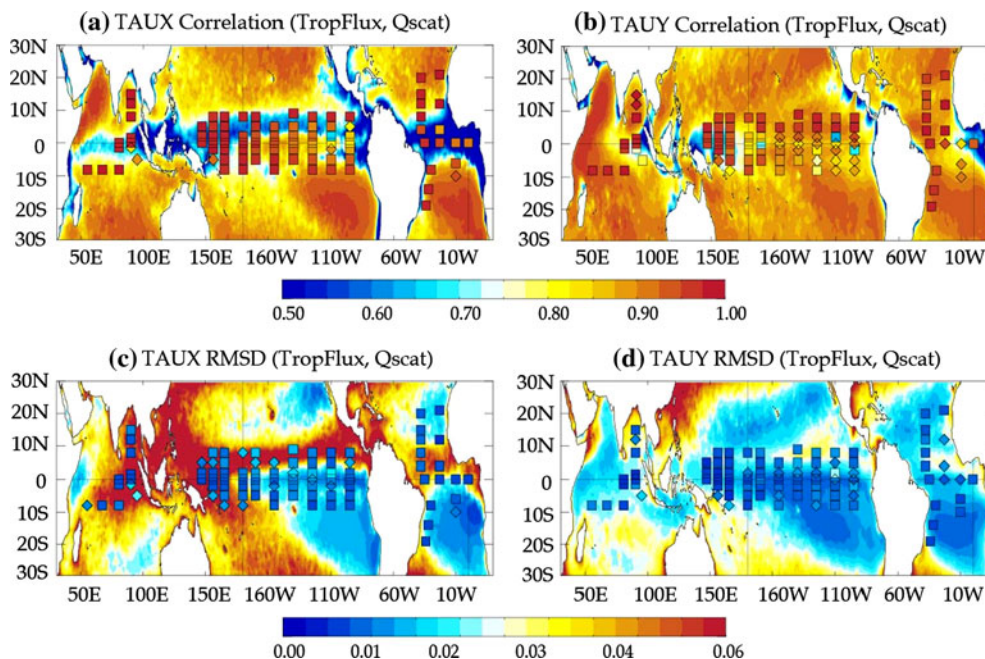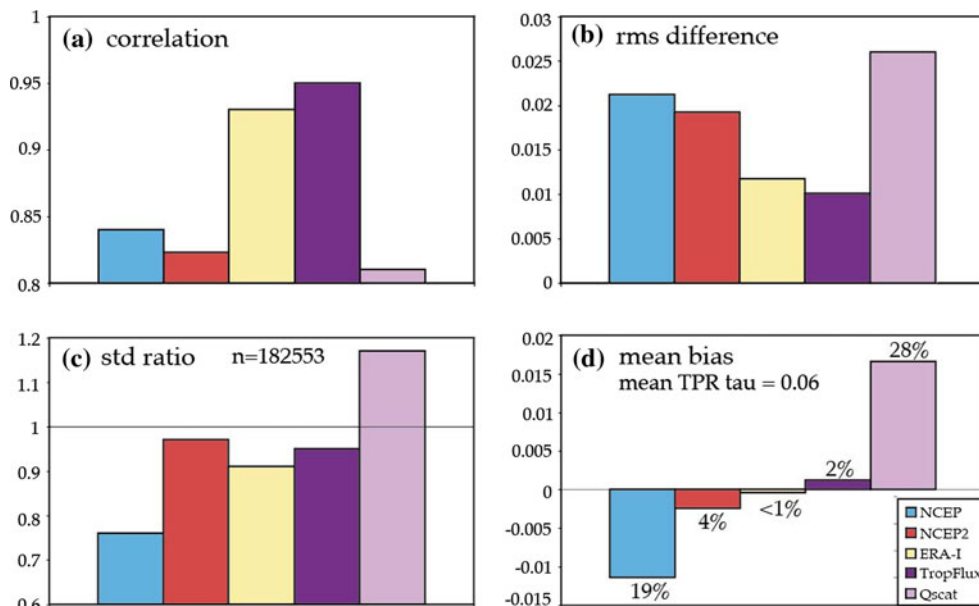
Fig. 5 Maps of correlation (**a, b**) and root mean square differences (**c, d**) between TropFlux and QuikSCAT zonal (**a, c**) and meridional (**b, d**) wind stresses. The statistics are computed over the whole QuikSCAT period. The statistics of the comparison to TPR mooring is plotted with the *same color code* with a *symbol* at each site. A *square* is used to indicate TPR site whenever the evaluation statistic of the TropFlux product is the best (i.e. highest correlation, lowest rms-difference) among NCEP, NCEP2, ERA-I and QuikSCAT; a *diamond* is used otherwise. TropFlux displays the highest correlation to TPR data for zonal wind stress at 84 sites out of 90 locations (66 out of 90 for meridional wind stress). It has the lowest rms-difference at 73 sites for zonal wind stress (71 for meridional wind stress)

The overall correlation of net heat flux to TPR data ranges from 0.54 (NCEP and NCEP2) to 0.87 (TropFlux) (Praveen Kumar et al. 2012). Our results clearly show that the agreement of wind stress products to TPR data is generally better than that for net heat flux, with correlations ranging from 0.82 (NCEP2 and QuikSCAT) to 0.95 (TropFlux).

4.2 Comparison of TropFlux and QuikSCAT products

The evaluation presented above is quite local in space. In order to provide an assessment in the entire tropical band, background colors in Fig. 5 show correlations and rms-differences of TropFlux to QuikSCAT wind stresses, over
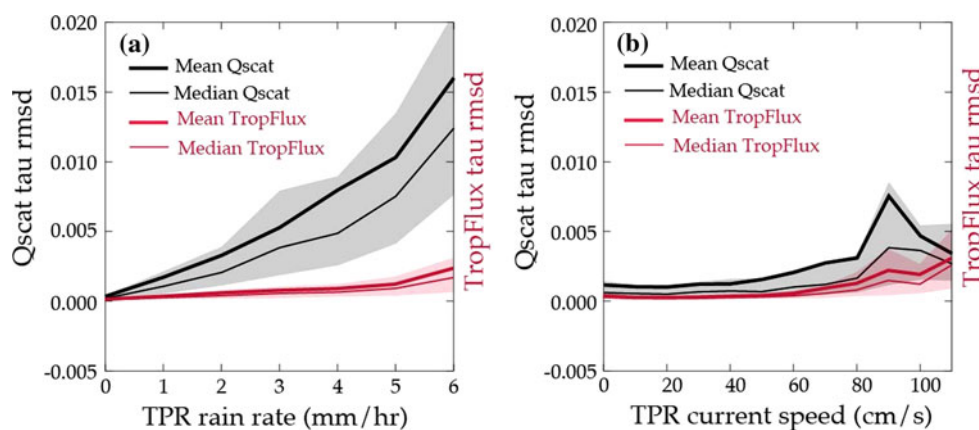
Fig. 6 Average (*thick curves*) and median (*thin curves*) root mean square difference between QuikSCAT (*black/grey*) and TropFlux (*red*) and TPR mooring wind stresses, as a function of TPR **a** rain rates and **b** current speed. The *shading* delineates the 1st and 3rd quartiles of the root-mean-square difference. In order to obtain these statistics, the QuikSCAT and TropFlux differences with TPR wind stress data have been binned depending on the TPR-measured value of the rain rate (**a**) or current speed (**b**), when both were available. The bin size was taken as 1/2 of the overall standard deviation of rain (**a**) and currents (**b**). The TPR wind stress estimates used in this plot account for the effect of surface current on wind stress

the QuikSCAT period. While QuikSCAT is not a direct measurement (and relies on inversion of a backscatter signal), its high quality has been underlined many times (e.g., Figure 3 in Praveen Kumar et al. 2012, shows that QuikSCAT winds, despite some overestimation, generally compare well to TPR data).

Left panels of Fig. 5 show a strong disagreement of TropFlux and QuikSCAT zonal wind stresses along Intertropical Convergence Zones (ITCZ) of the three tropical oceans, and to a lesser extent in the South Pacific Convergence Zone (SPCZ). At those locations, comparison with TPR data display much more favourable statistics for TropFlux (markers on Fig. 5a and c). As already mentioned, numerous studies already illustrate the inability of QuikSCAT to satisfactorily capture wind in rainy regions (Milliff et al. 2004; Gille 2005; Bentamy et al. 2012) due to backscatter of the radar signal by rain drops in the atmospheric column. Other authors (Bentamy et al. 2003; Chelton and Freilich 2005) however argue that scatterometers have the advantage of directly providing an estimate of stress at the ocean surface, hence naturally accounting for the influence of ocean currents on surface stress. We thus need to evaluate whether differences between TropFlux and QuikSCAT in Fig. 5 are the results of rainfall bias in the QuikSCAT product or due to the stationary ocean assumption in the other products, including for TPR at sites that do not carry near-surface current meters. To that end, Fig. 6 shows a scatter-plot of the rms-difference (mean, median and quartile values) between TropFlux/QuikSCAT wind stresses and TPR estimates, as a function of the TPR-measured rain rate (Serra et al. 2001) and near-surface current speed. For this plot we used TPR wind stress estimates that account for the effect of surface currents (rather than those based on absolute wind speed alone). The QuikSCAT and TropFlux differences with

those TPR wind stress were then binned depending on the TPR-measured value of the rain rate (Fig. 6a) or current speed (Fig. 6b). The bin size was defined as 1/2 of the overall standard deviation for both rain and currents.

TropFlux wind stress errors display hardly any dependence on either rain rate (Fig. 6a) or surface currents (Fig. 6b). This indicates that rain or surface currents do not contribute strongly to TropFlux wind stress errors. On the other hand, QuikSCAT wind stress rms-error clearly increases with rain-rates, while this increase is much less obvious as a function of current speed. This is a very clear indication that QuikSCAT differences with mooring-estimated stresses are largely the result of contamination by rainfall, not of the effect of surface currents, consistent with the recent results of Bentamy et al. (2012). In their study, Bentamy et al. (2012) demonstrated that the overall error in QuikSCAT wind retrievals diminishes when a stricter flagging of rain events is applied. These caveats for QuikSCAT hence explain its lower quality in heavy rain regions, when compared with other products.

In most rain-free regions, QuikSCAT and TropFlux wind stresses generally agree reasonably well (with correlations exceeding 0.8 and rms-differences generally below 0.03 Nm^{-2}; Fig. 5). This result does not indicate that TropFlux is better or worse than QuikSCAT in these areas, but that the two products are consistent with no obvious flaws away from the area coved by TPR moorings.

4.3 Independent validation to OceanSITES data

As we mentioned in Sect. 2.3, TPR observations do not provide a completely independent validation because (a) TPR observations are assimilated in various re-analyses and (b) TPR observations are used for deriving ad-hoc

Fig. 7 *Bar diagrams* showing validation of daily wind stresses from different sources against independent data from five moorings. *Blue color* denotes NCEP, *red* denotes NCEP2, *yellow* denotes ERA-I, *purple* denotes TropFlux and violet denotes QuikSCAT. The length of available data at each location is described in the *text*. The *numbers* at the *bottom* of **d** represents the number of observations used (in years) for the validation. Note that we have averaged the statistics from the three locations at the Subduction site
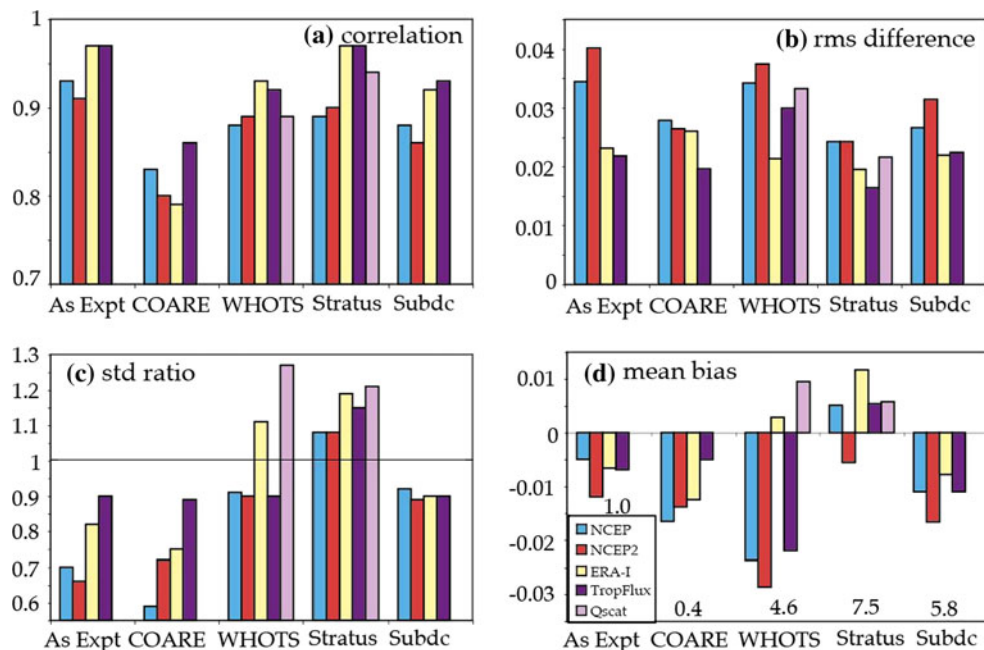
corrections while producing the TropFlux product. Data from the OceanSITES network are however neither used in re-analyses nor in the TropFlux generation procedure and hence provide an independent validation. Figure 7 summarizes the validation of wind stress magnitudes at the 5 mooring sites described in Sect. 2.3 (note that separate validation of the zonal and meridional components generally lead to the same conclusions).

The validation with independent data suggests that: (a) NCEP and NCEP2 generally underestimate mean wind stress and its variability (except at the stratus site), while other products have more differentiated behaviours; (b) TropFlux has 4 times out of 5 the highest correlation and 3 times out of 5 the lowest rms-difference, (c) there is generally (4 times out of 5) a neutral effect or improvement of TropFlux relative to ERA-I although this is not as clear as when gauged against TPR (also see Fig. 4). But overall, this validation relative to independent data suggests that TropFlux (and ERA-I) products generally provide the most accurate wind stress estimates in the tropics.

4.4 Differences in mean state

In this subsection, we briefly discuss climatological differences in wind stress. Figure 8 shows the long-term average wind stress for TropFlux (panel a), and the difference between all the other products and TropFlux (panels b–e). As shown in Fig. 8a, easterly winds clearly prevail in the Atlantic, Pacific and Southern Indian Oceans. The western Pacific and Indian Ocean warm-pool exhibit weak long-term mean wind stress. The Northern Indian Ocean annual average clearly exhibits the mark of the

Indian Monsoon flow, with a strong Somali jet over the Arabian Sea. ERA-I and TropFlux wind stress climatologies are very similar. In contrast, QuikSCAT tends to be much stronger than TropFlux everywhere, especially in the Pacific ITCZ. NCEP tends to be weaker in the 15°N–15°S band and NCEP2 stronger, except in the equatorial Pacific.

Wind stress curl is an important parameter for the ocean forcing outside of the equatorial waveguide. Contrasts between wind stress curl climatology amongst products are illustrated for the central Pacific in Fig. 9. In general, all display strong curl towards the center of subtropical gyres (between 20° and 30° of latitude), and slightly negative values between the equator and 10°S. All products display a maximum curl around 8–10°N associated with the boundary between the North Equatorial Current and North Equatorial Counter Current but with large discrepancies in both structure and amplitude. QuikSCAT has a double maximum structure, unlike any other products, probably related to rain contamination under the ITCZ (as discussed in Sect. 4.2) while NCEP maximum is much broader. The structure of maximum curl agrees reasonably well for NCEP2, TropFlux and ERA-I, with larger values for NCEP2 ($0.8 \ 10^{-7}$ instead of $\sim 0.5 \ 10^{-7}$ Pa m^{-1}).

Within the equatorial waveguide, the important dynamical quantity is zonal wind stress, rather than curl. The slope of the thermocline in the Pacific and Atlantic oceans is indeed to the first order in balance with the climatological zonal wind stress (e.g., McCreary 1981a, b). TPR data allows us to establish which products have the most realistic long-term estimate of wind stresses (Fig. 10) along the equatorial band. NCEP climatological equatorial wind stresses are too weak everywhere in the tropical band.

Fig. 8 a Long term
(2000–2008) annual mean wind
stress vectors (*arrows*) and
magnitude (*shading*) from
TropFlux. Differences between
the long term mean wind stress
magnitudes from **b** ERA-I, **c** the
QuikSCAT, **d** NCEP, **e** NCEP2
and TropFlux
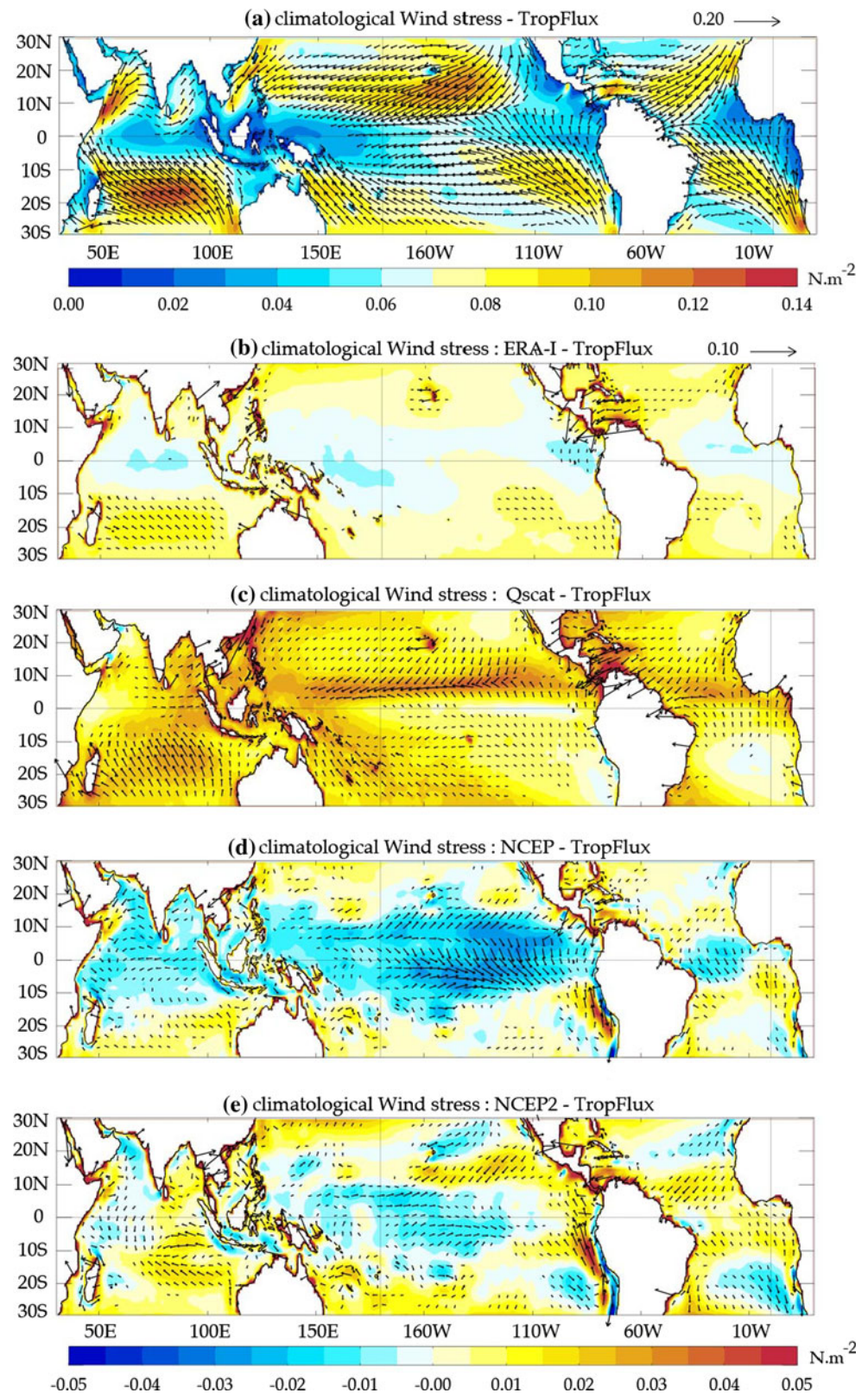
NCEP2 climatological equatorial wind stresses are too weak in the Pacific Ocean, but otherwise in close agreement with TPR. QuikSCAT climatological equatorial zonal wind stresses are overestimated by a large amount in the Indian Ocean and western Atlantic Ocean, but are generally similar to TPR in the Pacific. ERA-I and TropFlux display the best agreement with the TPR long-term average zonal equatorial wind stresses.
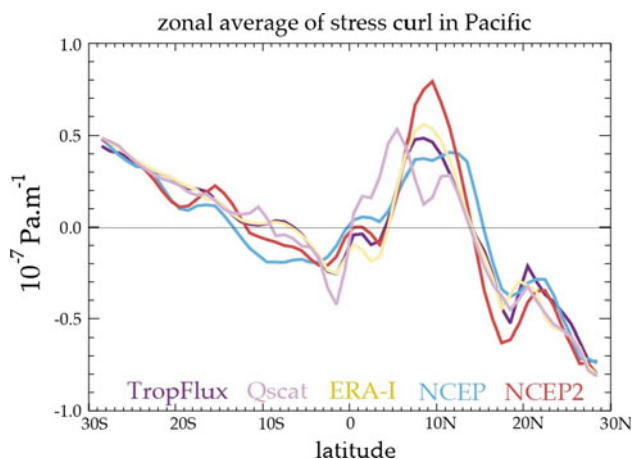
Fig. 9 Zonal average of wind stress curl in tropical Pacific (averaged between the dateline and 100°W) from different sources over 2000–2008

4.5 Intraseasonal, seasonal and interannual variability along the equatorial band

Zonal wind stress variations induce very clear ocean response at several timescales in the equatorial waveguide. On interannual timescales, this response is important dynamics in the Pacific Ocean for El Niño (e.g., Boulanger and Menkes 1999; Lengaigne et al. 2006), and in the Indian Ocean for the Indian Ocean Dipole (e.g., Le Blanc and

Boulanger 2001). On seasonal time-scales, the Indian Ocean displays a very energetic response to zonal wind stress, with very clear spring and fall jets (Wyrtki 1973). At intraseasonal timescale, there is also a clear modulation of equatorial currents and sea level in the Indian Ocean (e.g., Han et al. 2001; Sengupta et al. 2007; Nagura and McPhaden 2012). In the Pacific Ocean, intraseasonal wind variations induce a clear oceanic response (e.g., Cravatte et al. 2003), and westerly wind bursts (WWBs) in particular can contribute to the western displacement of the warm pool during the El Niño onset (Kessler et al. 1995; Lengaigne et al. 2002, 2004). In this section, we evaluate specifically zonal wind stresses to TPR data at each of those timescales. We define intraseasonal timescales as 10–90 day filtered data in order to retain both the influence of the MJO and WWBs. The seasonal cycle is defined by fitting three harmonics, and the interannual variability is defined as 90-day low-passed differences from the raw signal and the seasonal cycle.

Figure 11 shows intraseasonal statistics of zonal wind stress products along the entire equatorial strip. Observed zonal wind intraseasonal variability is strongest in the eastern Indian Ocean and in the western and Central Pacific (Fig. 11b), while it is comparatively small in the equatorial Atlantic. At this timescale, ERA-I and TropFlux products display the best agreement with TPR variability at almost all locations, both in terms of phase (with correlations >0.9

Fig. 10 a *Bar diagrams* of comparison between long-term mean zonal wind stress values from the TPR array with other products along the equator over the QuikSCAT period. The locations are mentioned in the *figure* and *numbers* in *brackets* correspond to the total number of available observations over the QuikSCAT period for evaluation (in years). **b** The mean zonal stress bias (product-TPR values) along the equator. TPR locations with a minimum of 365 valid observations over the QuikSCAT period are used to calculate the mean values
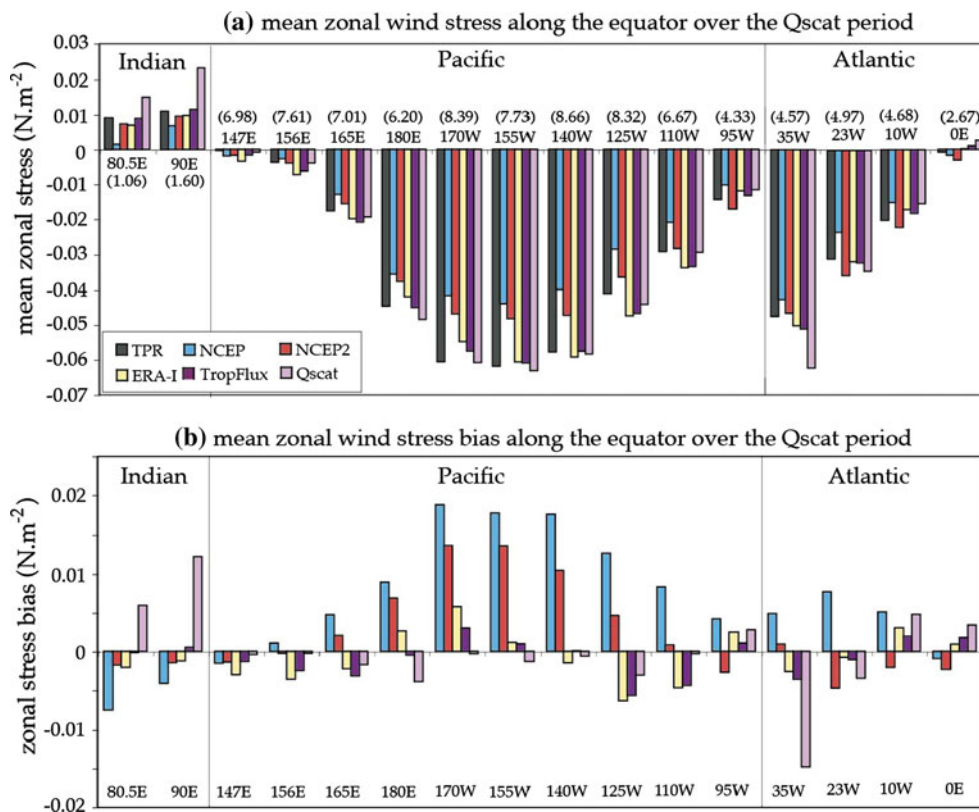
Fig. 11 *Bar diagrams* showing **a** correlation and **b** standard deviation ratio of intraseasonal (10–90 days filtered) zonal wind stress from various products compared to the TPR observations along the equator. In **b**, the observed 10–90 day standard deviation from TPR data is shown as a *grey shading* in the background (scale on the *right* of the plot). Different products are shown in *different colors*. Statistics are calculated over all the available valid data from TPR array over 1990–2010 period except for QuikSCAT. For QuikSCAT statistics are calculated over the entire QuikSCAT period. Note that similar results are obtained for other products when statistics are calculated over QuikSCAT period

(a) intraseasonal (10-90 day) taux correlation

(b) intraseasonal (10-90day) taux standard deviation and its ratio
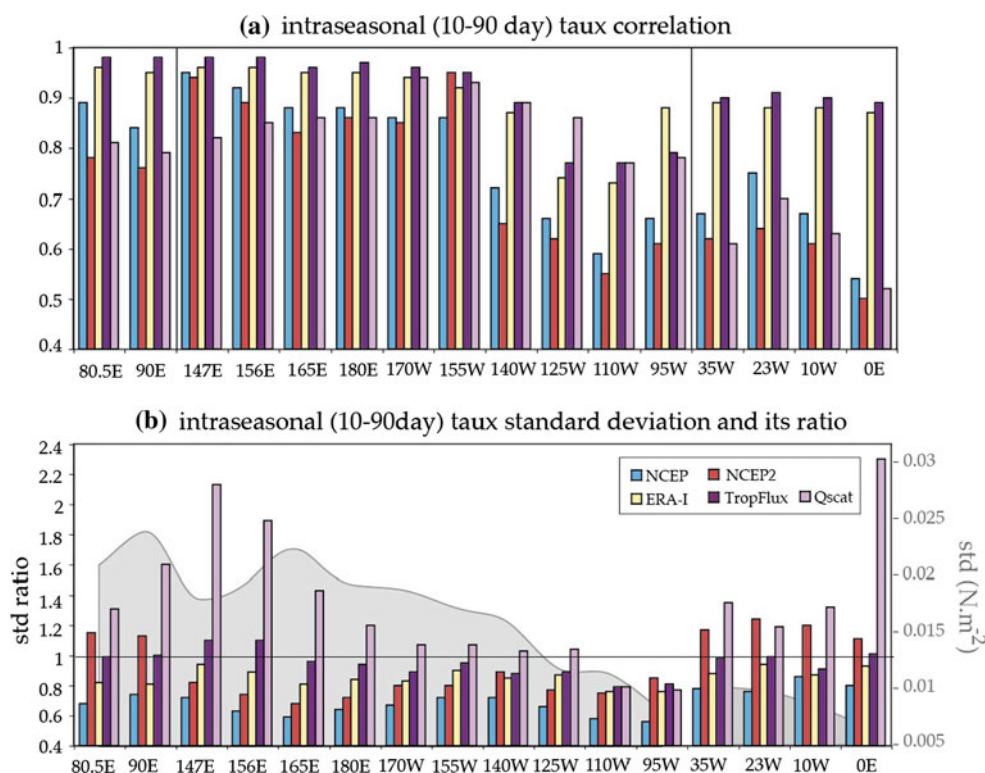
in the region of significant intraseasonal zonal wind stress variability, versus 0.8 at best for other products; Fig. 11a) and amplitude (Fig. 11b). Indeed, QuikSCAT strongly overestimates intraseasonal variability in the Indian Ocean and western Pacific. Both NCEP re-analyses underestimate zonal wind stress variability in the western Pacific (by $\sim$20 to 30 %), but only NCEP re-analysis underestimates intraseasonal zonal wind stress variability in the Indian Ocean. The improvement of TropFlux compared to ERA-I, although modest, is systematic in terms of phase and even clearer in terms of amplitude: the TropFlux and TPR intraseasonal wind stress amplitudes match at most locations.

Westerly wind bursts in late 1996 and 1997 were very important in the 1997–1998 El Niño onset and development (e.g., McPhaden 1999; Vialard et al. 2001; Lengaigne et al. 2002, 2003). Figure 12 shows 10–90 day filtered wind stresses from TPR data and other products (except QuikSCAT, which was not available yet) at 156°E and 165°E in late 1996 and 1997. These longitudes were chosen because they exhibit some of the strongest wind stress variability along the equator. Only TropFlux captures the full magnitude (with slight overestimation) of WWBs during this period (Fig. 12). While the March 1997 WWB is reasonably well captured by most products at 165°E (Fig. 12b), the December 1996 WWB (Fig. 12a) and April–May 1997 WWB (Fig. 12b) are strongly underestimated by the NCEP and NCEP2 re-analyses (by 70 %) and to lesser extend by ERA-I (by 40 %). In contrast, these

WWBs are of comparable magnitude to TAO/Triton data in TropFlux.

Figure 13 shows 10–90 day filtered wind stresses in the eastern Indian Ocean (0°, 90°E). In November 2007 and April 2008, all products show $\sim$20 days long westerly anomalies (overestimated by NCEP2 and QuikSCAT), which force a strong intraseasonal pulse of the Wyrtki jet (e.g., Sengupta et al. 2007). QuikSCAT sometimes generate spurious variability, probably due to rainfall contamination (e.g., a very strong spurious burst in December 2007, an overestimated westerly wind event in July 2008, etc.).

Various products display non-negligible differences, mainly in terms of amplitude of the seasonal cycle along the equatorial band (Fig. 14). None of the products match the amplitude of the observed seasonal cycle in the western and Central Pacific; overall amplitude underestimation is $\sim$20 to 30 %, except for QuikSCAT which strongly overestimates the seasonal cycle in the western Pacific Warm Pool. The phase agreement with TPR data is generally very good (correlation >0.9, except for QuikSCAT and NCEP2 at a few locations). TropFlux and ERA-I are almost always the best products, with TropFlux slightly improving ERA-I seasonal wind stresses.

Figure 15 shows zonal wind stress statistics on interannual time scales at all TAO/TRITON sites along the equator. Largest interannual observed zonal wind stress variability is found over the warm pool between 156°E and 180°E. Over this region, most products display quite good

Fig. 12 Intraseasonally filtered (10–90 days) zonal wind stress from different products at **a** 0°N156°E and **b** 0°N165°E. The mooring timeseries is shown in *black*, TropFlux in *purple*, ERA-I in *yellow*, QuikSCAT in *violet*, NCEP in *blue* and NCEP2 in *red*
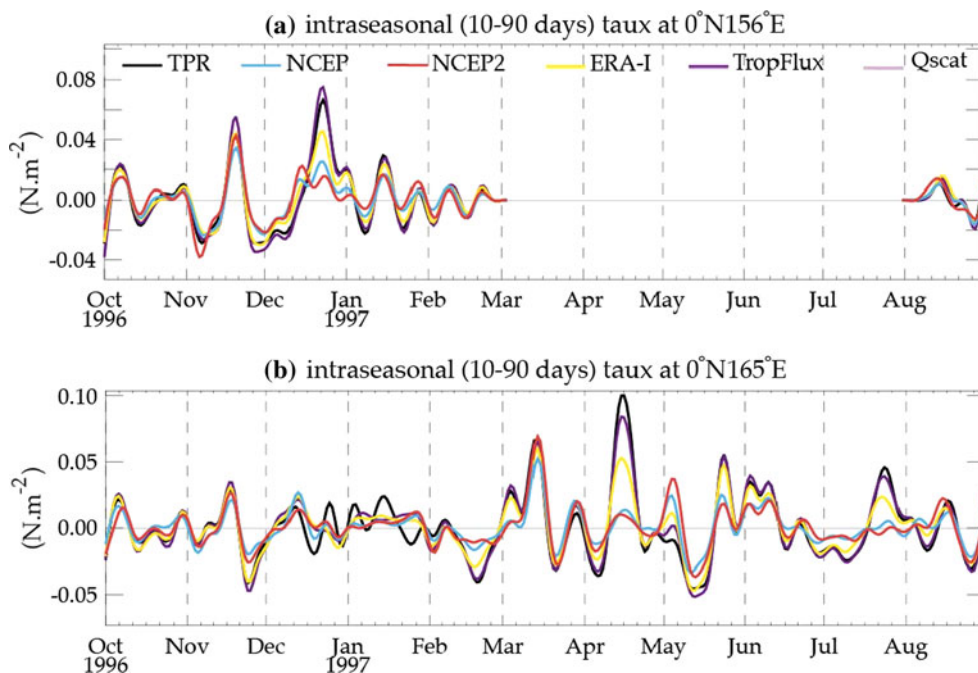
Fig. 13 Intraseasonally filtered (10–90 days) zonal wind stress from different products at 0°N90°E. The mooring timeseries is shown in *black*, TropFlux in *purple*, ERA-I in *yellow*, QuikSCAT in *violet*, NCEP in *blue* and NCEP2 in *red*
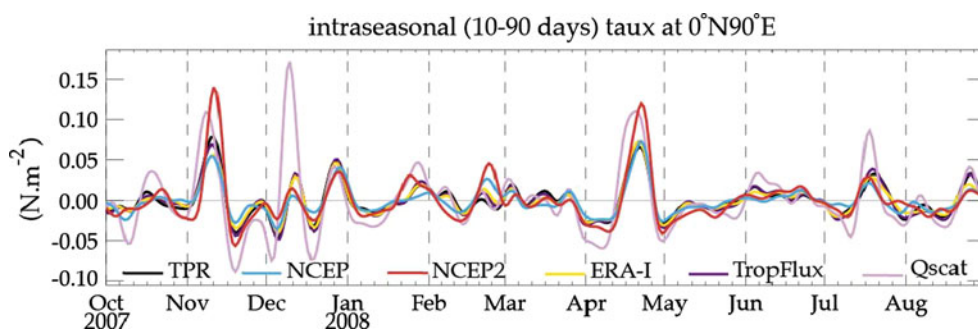
phase agreement with TPR zonal stresses (correlation >0.9). Most products, except TropFlux and QuikSCAT, tend to underestimate the interannual variability. TropFlux and ERA-I zonal wind stresses have the best interannual variability, with TropFlux displaying better amplitude agreement with TPR. In summary, statistics computed for the entire TPR network and for both components of the wind stresses (not shown) indicate that TropFlux and ERA-I display the best agreement with TPR data for the three timescales (intraseasonal/seasonal/interannual) within the entire tropical region.

4.6 Synthesis and comparison with heat fluxes

We define the following metric, e, in order to measure the level of agreement between various products X_i^j (where i designates one of the 5 wind stress products NCEP, NCEP2, ERA-I, TropFlux and QuikSCAT; j designates the 5-days time step):

$$e = \frac{\frac{1}{I}\sqrt{\sum_j \sum_i \left(X_i^j - \overline{X^j} - [X]\right)^2}}{\sqrt{\sum_j \left(\overline{X^j} - [X]\right)^2}} \text{ with } \overline{X^j} = \frac{1}{I}\sum_i X_i^j \text{ the "ensem-}$$

ble mean" of the I available products and $[X] = \frac{1}{IJ}\sum_j \sum_i X_i^j$ the ensemble average long term mean. The denominator of this expression is the standard deviation of the ensemble average of the 5 products and the numerator is the "ensemble spread", i.e. a root mean square measure of the spread around the ensemble mean $\overline{X^j}$. The "relative spread" e is a dimensionless quantity that expresses the typical spread of the products relative to the consensus value provided by the average of all products, and normalized by the variability of this consensus value. Note that this quantity does not measure systematics biases, only differences in variability.

We already noted that the agreement between various wind stress products and TPR data is in general better than for net heat fluxes discussed in Praveen Kumar et al. (2012) (correlations of 0.8–0.95 for wind stresses against 0.5–0.85 for heat fluxes). Figure 16 allows a quantitative comparison

Fig. 14 *Bar diagrams* showing **a** correlation and **b** standard deviation ratio of the long-term mean seasonal cycle zonal wind stress from various products compared to the TPR observations along the equator. In **b**, standard deviation of the observed seasonal cycle from TPR data is shown as a *grey shading* in the background (scale on the *right* of the plot). Different products are shown in *different colors*. Statistics are calculated over all the available valid data from TPR array over 1990–2010 period except for QuikSCAT. Locations with a minimum of 4 years of TPR data are used for this analysis. For QuikSCAT, statistics are calculated over the entire QuikSCAT period. Note that similar results are obtained for other products when statistics are calculated over QuikSCAT period
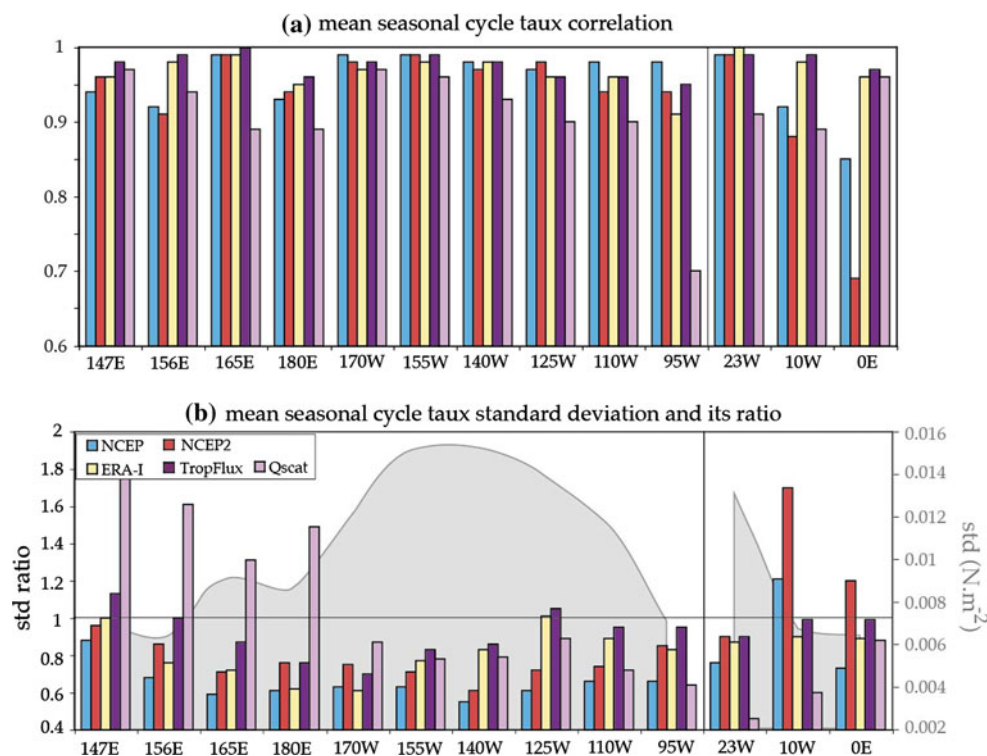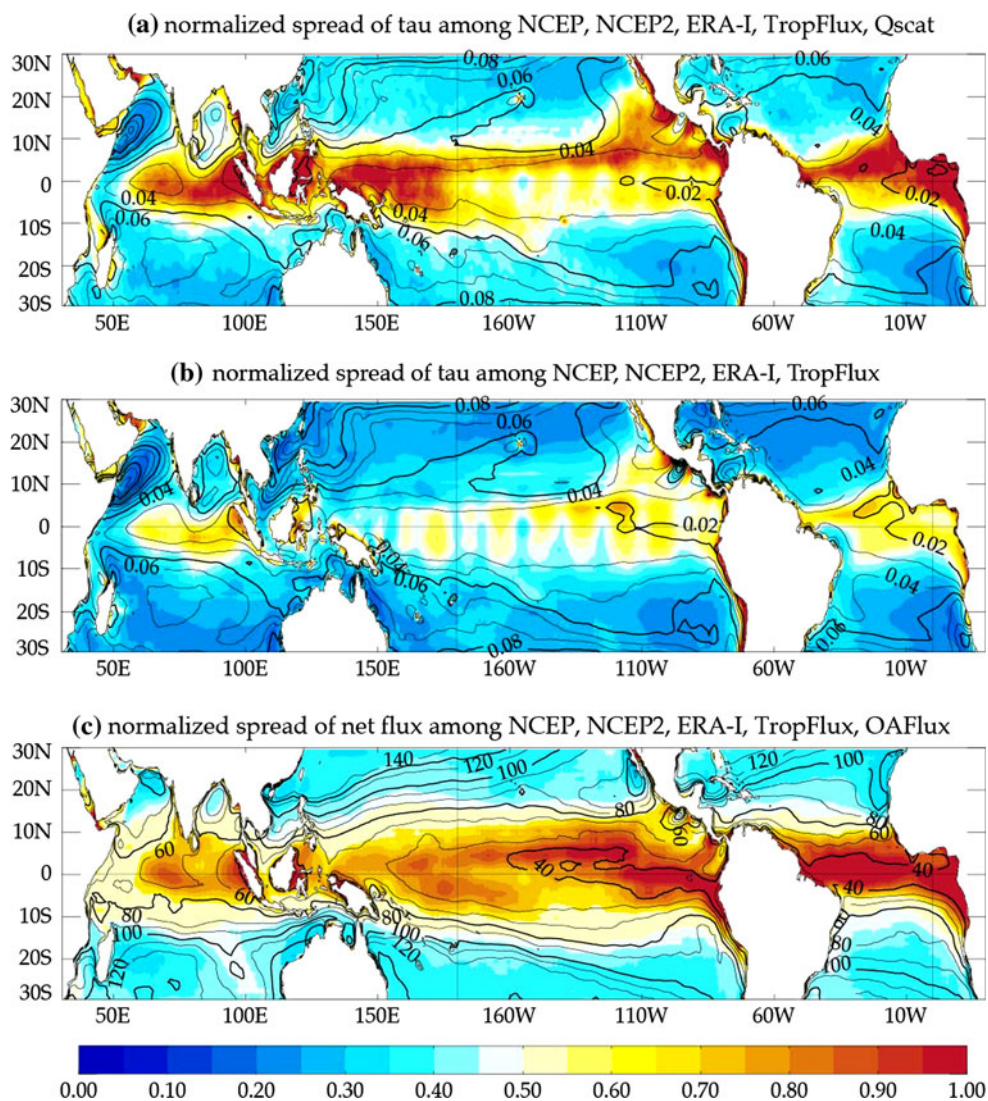

Fig. 15 *Bar diagrams* showing **a** correlation and **b** standard deviation ratio of interannual zonal wind stress from various products compared to the TPR observations along the equator. In **b**, standard deviation of the observed interannual stresses from TPR data is shown as a *grey shading* in the background (scale on the *right* of the plot). Different products are shown in *different colors*. Statistics are calculated over all the available valid data from TPR array over 1990–2010 period except for QuikSCAT. Locations with a minimum of 7 years of high quality TPR data are used for this statistics. For QuikSCAT statistics are calculated over the entire QuikSCAT period. Note that similar results are obtained for other products when statistics are calculated over QuikSCAT period
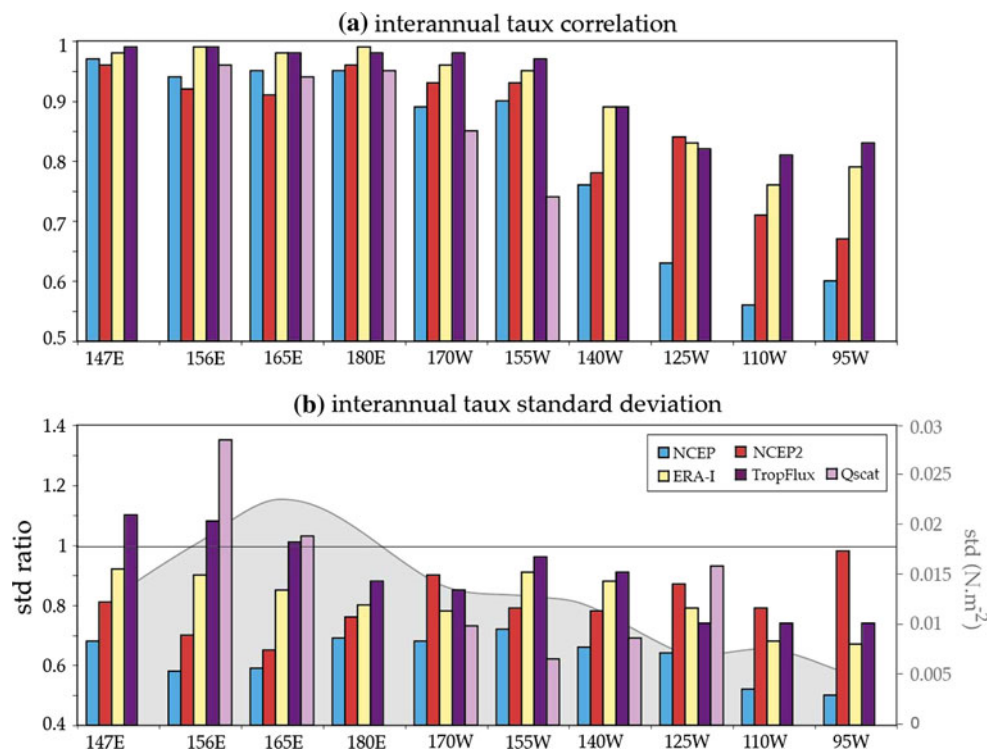
of the "relative spread" *e* of the 5 wind stress products in this study with the "relative spread" of the 5 net heat flux products in Praveen Kumar et al. (2012). Since the definition of this measure is relative to the amplitude of variability, both wind stress and net heat fluxes display stronger spread of values near the equator, where air–sea momentum and heat fluxes vary less, than toward mid latitudes (Fig. 16). Because of previously discussed issues related to the wind stress retrieval in intense rainfall regions, Quik-SCAT is often an outlier under the ITCZ in the Pacific and Atlantic Oceans, and in the western Pacific and eastern Indian Ocean warm pool. As a result, Fig. 16a shows a large

Fig. 16 Ensemble spread (see *text* for details) of **a** wind stress magnitude from NCEP, NCEP2, ERA-I, TropFlux and QuikSCAT, **b** wind stress magnitude from NCEP, NCEP2, ERA-I and TropFlux and **c** net heat flux from NCEP, NCEP2, ERA-I, OAFlux and TropFlux. The *contours* show the standard deviation of the average of the products

(a) normalized spread of tau among NCEP, NCEP2, ERA-I, TropFlux, Qscat

(b) normalized spread of tau among NCEP, NCEP2, ERA-I, TropFlux

(c) normalized spread of net flux among NCEP, NCEP2, ERA-I, TropFlux, OAFlux

spread under intense rainfall regions. This spread is strongly reduced when QuikSCAT is excluded from the spread computation (compare Fig. 16a, b; no equivalent reduction in spread is obtained when any other product is excluded). The normalized wind stress spread in Fig. 16b is overall clearly smaller than the spread of net heat fluxes (Fig. 16c, the zonal average flux spread is ∼0.85 at the equator and ∼0.4 poleward of 15° versus ∼0.55 and 0.3, respectively, for wind stress). This indicates that wind stress products agree better amongst themselves than net heat flux products. We will discuss this further in Sect. 5.

5 Summary and discussion

5.1 Summary

This paper is part of our ongoing effort to provide timely and accurate daily fluxes of heat and momentum over the global tropical oceans. We presented the TropFlux heat flux data in Praveen Kumar et al. (2012). Here, we present TropFlux wind stresses, available at 1° × 1°, daily resolution within 30°S–30°N from 1979 to almost near real time, from http://www.locean-ipsl.upmc.fr/tropflux and http://www.nio.org. Following Praveen Kumar et al. (2012), TropFlux wind stresses are computed by applying the COARE v3.0 algorithm to bias and amplitude corrected ERA-I data. A gustiness correction is also applied to wind speed on the basis of climatological SST, in order to account for unresolved (meso-scale, diurnal and subdiurnal) wind variations by the ERA-I dataset.

The resulting wind stresses as well as three other timely, daily re-analyses (ERA-I, NCEP and NCEP2), and the widely used QuikSCAT 1999–2009 wind stresses, are evaluated against dependent data from the TAO/TRITON, PIRATA and RAMA and independent OceanSITES mooring networks. Wind stress products are more consistent amongst each other than surface heat fluxes,

suggesting 10 m-winds are better constrained than near-surface thermodynamical parameters (2 m-humidity and temperature) and surface downward radiative fluxes. NCEP, NCEP2 and QuikSCAT wind stresses display equivalent overall performance relative to TPR data (correlations of 0.81–0.84 and rms-differences of 0.021–0.026 Nm^{-2}). QuikSCAT overestimates wind stresses away from the equator, while NCEP and NCEP2 underestimate wind stresses. QuikSCAT zonal wind stress quality is strongly affected by rain under the ITCZ. Both ERA-I and TropFlux display the best agreement with in situ data, with correlations >0.93 and rms-differences <0.012 Nm^{-2}. The TropFlux wind stresses exhibit a small, but consistent improvement (at various timescales and most locations) over ERA-I, with an overall 17 % reduction in rms-error.

We further investigate equatorial zonal wind stresses in detail, owing to their importance for forced ocean dynamical responses. NCEP climatological equatorial wind stresses are too weak everywhere in the tropical band. NCEP2 climatological equatorial wind stresses are too weak in the Pacific Ocean, but otherwise in good agreement with TPR. QuikSCAT climatological equatorial zonal wind stresses are overestimated by a large amount in the Indian Ocean and western Atlantic Ocean, but are generally more accurate in the Pacific. ERA-I and TropFlux display the best agreement with the TPR long-term average zonal equatorial wind stresses. All products tend to underestimate the zonal wind stress seasonal cycle by ~ 20 % in the western and central equatorial Pacific. Consistent with the overall statistics discussed earlier, TropFlux and ERA-I equatorial zonal wind stresses have clearly the best phase agreement to TPR data at intraseasonal and interannual timescales (correlation of ~ 0.9 vs. ~ 0.8 at best for any other product), with TropFlux correcting the ~ 13 % underestimation of ERA-I variability amplitude at both timescales.

While overall statistics indicate almost identical performances of ERA-I and TropFlux, these two products display significant differences on an event-to-event basis. For example, various products display important differences in reproducing the late 1996 and 1997 westerly wind bursts that played a key role in the 1997–1998 El Niño onset and development, with TropFlux displaying the best agreement to TPR data.

Finally, Table 1 provides a quantitative estimate of the rms-errors of TropFlux with respect to TPR data: 0.009 Nm^{-2} for 5-day averaged data, a value that does not vary strongly depending on the basin. The average root-mean-square wind stress magnitude at all TPR sites is 0.061 Nm^{-2} for both TPR and TropFlux. This provides a relative measure of the uncertainty in the TropFlux wind stress product: 0.009/0.061, i.e. a 15 % error arising from sampling and observational uncertainties. This number can be compared with the 5–10 % accuracy of the COARE

Table 1 Evaluation statistics of TropFlux wind stress magnitude against high-quality TPR mooring observations over the QuikSCAT period

	Cor	Bias (Nm^{-2})	Std ratio	rms-error (Nm^{-2})
Global (daily)	0.92	0.000	0.93	0.013
Global (5-day)	0.95	0.003	0.95	0.009
Indian ocean	0.97	0.001	0.98	0.008
Pacific ocean	0.94	0.005	0.94	0.010
Atlantic ocean	0.95	0.003	0.95	0.010

The first rows of values are statistics for daily data; the rest are for 5-day smoothed data. Statistical quantities are correlation, TropFlux minus TPR bias, standard deviation of TropFlux divided by standard deviation of TPR, and root-mean-square error of TropFlux to the TPR. In order to obtain estimates of the percentage of accuracy of pentad TropFlux wind stress estimates, the rms-error should be divided by the average root-mean-square value of TPR wind stress magnitude of 0.061 Nm^{-2} (the value for TropFlux is very close)

algorithm quoted by Fairall et al. (2003). If instrumental and sampling errors are assumed to be independent from errors arising from the use of a bulk transfer coefficient, the typical error on the 5-day averaged TropFlux wind stress estimates is hence below 20 %, and mostly arises from wind and sampling uncertainties.

5.2 Discussion and perspectives

This study suffers from the same limitation as that of Praveen Kumar et al. (2012). First, we use dependent data from the TPR array extensively and so our evaluation is more a check on the ability of the various products to fit the observations than a true independent validation. We do, however, believe that the most serious issue associated with the use of these data is the fact that our analysis is most complete in the well-sampled 10°N–10°S latitude band best sampled by the TPR array: we trust our evaluation of the various products within this band, but it is probably less representative of the 10°–30° band.

Another limitation of our study is that we rely on the TPR wind stress estimates, and hence on the COARE v3.0 algorithm, and the gustiness approach proposed by Cronin et al. (2006). COARE has been developed specifically for tropical regions and Fairall et al. (2003) claim a 5–10 % accuracy of the COARE algorithm for winds up to 20 ms^{-1}. In addition, the gustiness approach proposed by Cronin et al. (2006) (but applied here over the entire TPR array) is based on actual climatological differences between wind speeds estimated from daily averages, and wind speeds estimated from high frequency (10 min) data. One of the limitations of our approach, however, is that this application of the gustiness is climatological, and does not take into account non-seasonal variations of the convective and meso-scale variability.

Another possible limitation of our method is that we neither account for the effect of surface waves nor surface currents in the computation of the wind stress (surface waves act mainly by modifying the ocean's surface roughness, and surface currents by influencing the relative speed of air with respect to the sea). Some studies have pointed out that the effect of currents and waves may not be negligible for wind stress estimates (e.g., Dawe and Thompson 2006; Kara et al. 2007). We however feel that our approximations do not cause large errors in the Trop-Flux dataset. Regarding the effect of surface currents, the TPR product accounts for the effect of surface currents when available and Fig. 6 clearly shows that large observed surface currents are not a source of large error in TropFlux compared to TPR. The situation is more difficult regarding surface waves. We don't have available in situ wave characteristics estimates at TPR mooring sites to evaluate the effect of waves from in situ data. Fairall et al. (2003) however noted that "*the wave stress community lacked consensus on how to handle waves*" when estimating wind stress. Despite those two difficulties, we have two hints that the effects of waves may not be of first-order importance in the tropics. First, ERA-I stresses include explicitly the effect of waves on stress through an interactive wave model, and ERA-I wind stresses are not very different from Trop-Flux. Second, the COARE v3.0 algorithm includes two parameterizations of the effect of waves (Oost et al. 2002; Yelland and Taylor 1996) as a function of the dominant wave period (Oost et al. 2002) and of significant wave height (Yelland and Taylor 1996), both of which we obtained from the ERA-I re-analysis. Re-computing the TropFlux product with those two estimates yields differences that are typically smaller than the differences between TropFlux and most other products (NCEP, NCEP2, Quik-SCAT, not shown). We have hence not included these wave parameterizations in the current TropFlux product, but we recognize the need for a more thorough investigation of the effects of surface waves and surface currents in a future study. While these two effects are generally not large in the equatorial strip, they may be non negligible in strong surface currents and very strong wind conditions, as, e.g., in the western Arabian Sea during the monsoon (e.g., Schott and McCreary. 2001) or in intense tropical storms.

Results from other studies assessing wind stress are generally consistent with ours. Jiang et al. (2005) compare various wind speed products with TPR data, and find consistent results: NCEP and NCEP2 tend to underestimate wind speed, and QuikSCAT tends to overestimate it away from the equator. Jiang et al. (2008) compare an ocean general circulation model forced by NCEP2 and Quik-SCAT wind stresses. They show an improvement of the model mean state when QuikSCAT wind stresses are used, but no discernable improvement of intraseasonal SST and thermocline depth variations. This last result is qualitatively consistent with the results of Fig. 11, which indicate a comparable correlation of NCEP2 and QuikSCAT to TPR data at intraseasonal timescale. Meissner et al. (2001) and Josey et al. (2002) also indicate that NCEP wind stresses tend to be underestimated in the tropical region. Studies by Chelton and Freilich (2005), Milliff et al. (2004), Gille (2005), Bentamy et al. (2012) also point to a tendency of QuikSCAT to overestimate winds (and wind stresses) and indicate deficiencies of this dataset in intense rainfall regions.

Our results outline some issues with the use of Quik-SCAT wind stress data in rainy regions (where it clearly appears as an outlier amongst the products, see Figs. 10 and 16). Scatterometer data is still useful though. Many re-analyses and operational products assimilate scatterometer data, with appropriate bias correction and flagging of incorrect data, and this contributes to improving the estimation of surface wind stress (e.g., Chelton et al. 2006), especially in the many oceanic regions where no other direct information on surface wind is available. In addition, the QuikSCAT wind stresses are often of superior quality to some re-analyses (NCEP and NCEP2) away from rainy regions. Many studies of ocean dynamical response to wind stress forcing however use QuikSCAT wind stresses (e.g., Sengupta et al. 2007, Nagura and McPhaden 2010a, b; Cravatte et al. 2007; Jiang et al. 2009, amongst many others). We note that, for studies of equatorial ocean dynamics, the ERA-I or TropFlux wind stress forcing are however more appropriate, because they resolve intraseasonal and interannual variability much better in the important forcing regions (e.g., the eastern Indian Ocean and western Pacific), and do not suffer from rainfall contamination as does QuikSCAT.

Our results indicate that wind stresses are generally better constrained than heat fluxes (less spread amongst products, and better consistency with mooring data). This can probably be explained by the fact that wind stress computation largely relies on 10 m wind estimation (2 m-temperature and humidity only have a weak impact, through the drag coefficient computation), which are better constrained by the observing system than surface thermodynamical parameters. Scatterometers indeed provide wide-coverage information about surface winds, while there is no equivalent data for surface humidity and temperature. In addition, wind is also constrained by numerous pressure measurements through geostrophic balance constraints in assimilation systems. As a result, winds suffer from relatively lower systematic biases than surface temperature and humidity (Praveen Kumar et al. 2012). Finally, surface radiative fluxes are a strong source of error in net surface heat fluxes (Praveen Kumar et al. 2012). This is probably due to the fact that, while assimilation systems

assimilate Outgoing Longwave Radiation (i.e. longwave emission at the top of the atmosphere), they do not impose much constraint on the surface heat budget.

One obvious application of surface heat and wind stress products is to force ocean models. The current study suggests that for tropical studies, the ERA-I and TropFlux data provide very high quality wind stresses and, depending on the particular application, should be preferred to other possibilities. As far as net heat fluxes are concerned, Praveen Kumar et al. (2012) however underlined the ERA-I systematic biases (too strong oceanic heat losses by ~ 15 Wm^{-2}), and errors in shortwave fluxes (resulting in an overall correlation to TPR of ~ 0.75 against ~ 0.83 for TropFlux net heat fluxes). Studies also concerned with thermodynamical response of the tropical ocean should hence use TropFlux fluxes, or apply correction strategies similar to those implemented in the Drakkar Forcing Set (Brodeau et al. 2010).

The TropFlux surface meteorological parameters, surface heat fluxes and wind stress data are available on the TropFlux website at http://www.locean-ipsl.upmc.fr/tropflux from 1979 to nearly the present with daily resolution on a 1° grid. We are currently working to automatically update TropFlux heat and momentum fluxes so that they are no more than 4 months delayed from the present. We hope that our efforts to develop a better heat and momentum flux product for the tropical oceans will lead to new insights into tropical ocean–atmosphere interactions and tropical climate variability.

References

Annamalai H, Murtugudde R, Potemra J, Xie SP, Liu P, Wang B (2003) Coupled dynamics over the Indian Ocean: spring initiation of the zonal mode. Deep Sea Res II 50:2305–2330

Bentamy A, Quilfen Y, Gohin F, Grima N, Lenaour M, Servain J (1996) Determination and validation of average wind fields from ERS-1 scatterometer measurements. Glob Atmos Ocean Syst 4:1–29

Bentamy A, Katsaros KB, Alberto M, Drennan WM, Forde EB (2002) Daily surface wind fields produced by merged satellite data. Am Geophys Union Geophys Monogr Ser 127:343–349

Bentamy A, Katsaros KB, Mestas-Nuñez AM, Drennan WM, Forde EB, Roquet H (2003) Satellite estimates of wind speed and latent heat flux over the global oceans. J Climate 16:637–656

Bentamy A, Grodsky SA, Carton JA, Croizé-Fillon D, Chapron B (2012) Matching ASCAT and QuikSCAT winds. J Geophys Res 117:C02011. doi:10.1029/2011JC007479

Bjerknes J (1966) A possible response of the atmospheric Hadley circulation to equatorial anomalies of ocean temperature. Tellus 18:820–829

Boulanger J-P, Menkes C (1999) Long equatorial wave reflection in the Pacific Ocean from TOPEX/POSEIDON data during the 1992–1998 period. Clim Dyn 15:205–225

Bourlès B, Lumpkin R, McPhaden MJ, Hernandez F, Nobre P, Campos E, Yu L, Planton S, Busalacchi AJ, Moura AD, Servaom J, Trotte J (2008) The PIRATA program: history, accomplishments and future directions. Bull Am Meteorol Soc 89:1111–1125

Brink NJ, Moyer KA, Trask RP, Weller RA (1995) The subduction experiment: mooring field program and data summary. Woods Hole Oceanographic Institution. WHOI-95-08

Brodeau L, Barnier B, Penduff T, Treguier AM, Gulev S (2010) An ERA-40 based atmospheric forcing for global ocean circulation models. Ocean Model 31:88–104. doi:10.1016/j.ocemod.2009.10.005

Bruke MA, Fairall CW, Zeng X, Eymard L, Curry JA (2003) Which bulk aerodynamic algorithms are least problematic in computing ocean surface turbulent fluxes? J Clim 16(4):619–635

Bunker AF (1976) Computations of surface energy flux and annual air-sea interaction cycles of the north Atlantic. Mon Weather Rev 104:1122–1140

Cassou C (2008) Intraseasonal interaction between the Madden–Julian Oscillation and the North Atlantic Oscillation. Nature 455:523–527

Chelton DB, Freilich MH (2005) Scatterometer based assessment of 10-m wind analyses from the operational ECMWF and NCEP numerical weather prediction models. Mon Weather Rev 133:409–429

Chelton DB, Freilich MH, Sienkiewicz JM, Von Ahn JM (2006) On the use of QuikSCAT scatterometer measurements of surface winds for marine weather prediction. Mon Weather Rev 134:2055–2071

Colbo K, Weller R (2007) The variability and heat budget of the upper ocean under the Chile-Peru stratus. J Mar Res 65:607–637

Cravatte S, Picaut J, Eldin G (2003) Second and first baroclinic Kelvin modes in the equatorial Pacific at intraseasonal time-scales. J Geophys Res 108:3266. doi:10.1029/2002JC001511

Cravatte S, Madec G, Izumo T, Menkes C, Bozec A (2007) Progress in the 3-D circulation of the eastern equatorial Pacific in a climate ocean model. Ocean Model 17:28–48

Cronin MF, Fairall C, McPhaden MJ (2006) An assessment of buoy-derived and numerical weather prediction surface heat fluxes in the tropical Pacific. J Geophys Res 111:C06038. doi:10.1029/2005JC003324

da Silva AM, Young CC, Levitus S (1994) Algorithms and procedures. Vol 1,. Atlas of surface marine data. NOAA Atlas NESDIS 6

Dawe JT, Thompson L (2006) Effect of ocean surface currents on wind stress, heat flux, and wind power input to the ocean. Geophys Res Lett 33:L09604. doi:10.1029/2006GL025784

Dee DP et al (2011) The ERA-Interim reanalysis: configuration and performance of the data assimilation system. Q J R Meteorol Soc 137(553):597. doi:10.1002/qj.828

Drushka K, Sprintall J, Gille ST, Wijffels W (2011) In situ observations of Madden-Julian Oscillation mixed layer dynamics in the Indian and Western Pacific Oceans. J Clim. doi:10.1175/JCLI-D-11-00203.1

Duvel J-P, Vialard J (2007) Indo-Pacific sea surface temperature perturbations associated with intraseasonal oscillations of the tropical convection. J Clim 20:3056–3082

Fairall CW, Bradley EF, Rogers DP, Edson JB, Young GS (1996) Bulk parameterization of air-sea fluxes for tropical ocean-global atmosphere coupled ocean-atmosphere response experiment. J Geophys Res 101:3747–3764

Fairall CW, Bradley EF, Hare JE, Grachev AA, Edson JB (2003) Bulk parameterization on air-sea fluxes: updates and verification for the COARE algorithm. J Climate 16:571–591

Freitag HP, McCarty ME, Nosse C, Lukas R, McPhaden MJ, Cronin MF (1999) COARE Seacat data: calibrations and quality control procedures. NOAA Tech. Memo. ERL PMEL-115

Freitag HP, O'Haleck M, Thomas GC, McPhaden MJ (2001) Calibration procedures and instrumental accuracies for ATLAS wind measurements. NOAA. Tech. Memo. OAR PMEL-119, NOAA/Pacific Marine Environmental Laboratory, Seattle, Washington

Gille ST (2005) Statistical characterization of zonal and meridional ocean wind stress. J Atmos Ocean Technol 22:1353–1372

Hackert EC, Busalacchi AJ, Murtugudde R (2001) A wind comparison study using an ocean general circulation model for the 1997–98 El Niño. J Geophys Res 106:2345–2362

Han W, Lawrence DM, Webster PJ (2001) Dynamical response of equatorial Indian Ocean to intraseasonal winds: zonal flow. Geophys Res Lett 28:4215–4218

Han W, Meehl GA, Rajagopalan B et al (2010) Patterns of Indian Ocean sea-level change in a warming climate. Nat Geo sci 3:546–550. doi:10.1038/ngeo901

Han W, McCreary JP, Masumoto Y, Vialard J, Duncan B (2011) Basin modes in the equatorial Indian Ocean. J Phys Oceanogr 41:1252–1270

Hellerman S, Rosenstein M (1983) Normal monthly wind stress over the World Ocean with error estimates. J Phys Oceanogr 13:1093–1104

Huddleston JN, Stiles BW (2000) Multi dimensional histogram (MUDH) rain flag product description, Version 2.1. Jet Propulsion Laboratory, Pasadena

Jayakumar A, Vialard J, Lengaigne M, Gnanaseelan C, McCreary JP, Praveen Kumar B (2011) Processes controlling the surface temperature signature of the Madden-Julian Oscillation in the thermocline ridge of the Indian Ocean. Clim Dyn (online). doi:10.1007/s00382-010-0953-5

Jiang C, Cronin MF, Kelly KA, Thompson L (2005) Evaluation of a hybrid satellite- and NWP-based turbulent heat flux product using Tropical Atmosphere-Ocean (TAO) buoys. J Geophys Res 110(C9):C09007. doi:10.1029/2004JC002824

Jiang C-L, Thompson L, Kelly KA (2008) Equatorial influence of QuikSCAT winds in an isopycnal ocean model compared to NCEP2 winds. Ocean Model 24. doi:10.1016/j.ocemod.2008.05.003

Jiang C, Thompson L, Kelly KA, Cronin MF (2009) The roles of intraseasonal Kelvin waves and tropical instability waves in SST variability along the equatorial Pacific in an isopycnal ocean model. J Clim 22. doi:10.1175/2009JCLI2767.1

Josey S, Kent E, Taylor P (2002) Wind stress forcing of the ocean in the SOC climatology: comparisons with the NCEP-NCAR, ECMWF, UWM/COADS, and Hellerman and Rosenstein datasets. J Phys Oceanogr 32:1993–2019

Kalnay E et al (1996) The NCEP/NCAR 40-year reanalysis project. Bull Am Meteor Soc 77:437–470

Kanamitsu M, Ebisuzaki W, Woolen J, Potter J, Fiorino M (2002) NCEP/DOE AMIP-II Reanalysis (R-2). Bull Am Meteor Soc 83:1631–1643

Kara AB, Metzger EJ, Bourrassa MA (2007) Ocean current and wave effects on wind stress drag coefficient over the global ocean. Geophys Res Lett 34:L01604. doi:10.1029/2006GL027849

Kessler WS, McPhaden MJ, Weickmann KM (1995) Forcing of intraseasonal Kelvin Waves in the equatorial Pacific. J Geophys Res 100:10613–10631

Kessler WS, Johnson GC, Moore DW (2003) Sverdrup and nonlinear dynamics of the pacific equatorial currents. J Phys Oceanogr 33:994–1008

Kochanski A, Koracin D, Dorman CE (2006) Comparison of wind-stress algorithms and their influence on wind-stress curl using buoy measurements over the shelf off Bodega Bay, California. Deep-Sea Res II 53:2865–2886

Lake BJ, Norr SM, Freitag HP, McPhaden MJ (2003) Calibration procedures and intrumental accuracy estimates of ATLAS air temperature and relative humidity measurements. NOAA Tech Memo. OAR PMEL-123, NOAA/Pacific Marine Environmental Laboratory, Seattle

Large WG, Pond S (1981) Open ocean momentum flux measurements in moderate to strong winds. J Phys Oceanogr 11:324–336

Le Blanc J-L, Boulanger J-P (2001) Propagation and reflection of long equatorial waves in the Indian Ocean from TOPEX/POSEIDON data during the 1993–1998 period. Clim Dyn 17:547–557

Lee T, McPhaden MJ (2008) Decadal phase change in large-scale sea level and winds in the Indo-Pacific region at the end of the 20th century. Geophys Res Lett 35:L01605. doi:10.1029/2007GL032419

Lengaigne M, Boulanger J-P, Menkes C, Masson S, Madec G, Delecluse P (2002) Ocean response to the March 1997 westerly wind event. J Geophys Res 107:8015. doi:10.1029/2001JC000841

Lengaigne M, Boulanger J-P, Menkes C, Madec G, Delecluse P, Guilyardi E, Slingo J (2003) The March 1997 westerly wind event and the onset of the 1997/98 El Niño: understanding the role of the atmospheric response. J Clim 16:3330–3343

Lengaigne M, Boulanger JP, Delecluse P, Menkes C, Slingo J (2004) Westerly Wind Events and their influence on coupled ocean-atmosphere system: a review. Earth's climate: the ocean–atmosphere interaction. Am Geophys Union Geophys Monogr 147:49–69

Lengaigne M, Boulanger J-P, Menkes C, Spencer H (2006) Influence of the seasonal cycle on the termination of El Niño events in a coupled general circulation model. J Clim 19:1850–1868. doi:10.1175/JCLI3706.1

McCreary JP (1981a) A linear stratified ocean model of the coastal undercurrent. Philos Trans R Soc Lond 298:603–635

McCreary JP (1981b) A linear stratified ocean model of the coastal undercurrent. Phil Trans R Soc Lond 298:603–635

McPhaden MJ (1999) Genesis and evolution of the 1997–98 El Niño. Science 283:950–954

McPhaden MJ (2004) Evolution of the 2002/03 El Niño. Bull Am Meteor Soc 85:677–695

McPhaden MJ, Busalacchi AJ, Cheney R, Donguy JR, Gage KS, Halpern D, Ji M, Julian P, Mayers G, Mitchum GT, Niiler PP, Picaut J, Reynolds RW, Smith N, Takeuchi K (1998) The tropical ocean-global atmosphere (TOGA) observing system: a decade of progress. J Geophys Res 103:14169–14240

McPhaden MJ, Zebiak SE, Glantz MH (2006) ENSO as an integrating concept in Earth science. Science 314:1740–1745

McPhaden MJ, Meyers G, Ando K, Masumoto Y, Murty VSN, Ravichandran M, Syamsudin F, Vialard J, Yu W, Wu L (2009) RAMA: research moored array for african-asian-australian monsoon analysis and prediction. Bull Am Meteor Soc 90:459–480

McPhaden MJ, Ando K, Bourlès B, Freitag HP, Lumpkin R, Masumoto Y, Murty VSN, Nobre P, Ravichandran M, Vialard J, Vousden D, Yu W (2010) The global tropical moored buoy array. In: Hall J, Harrison DE, Stammer D (eds), Proceedings of the "OceanObs'09: sustained ocean observations and information for society" Conference (Vol 2), Venice, 21–25 September 2009, ESA Publication WPP-306

Medavaya M, Waliser DE, Weller RA, McPhaden MJ (2002) Assessing ocean buoy shortwave shortwave observations using clear-sky model calculations. J Geophys Res 107(C2):3014. doi:10.1029/2000JC000558

Meissner T, Smith D, Wentz F (2001) A 10 year intercomparison between collocated Special Sensor Microwave Imager oceanic surface wind speed retrievals and global analyses. J Geophys Res 106:11731–11742

Milliff RF, Morzel J, Chelton D, Freilich MH (2004) Wind stress curl and wind stress divergence biases from rain effects on QUIKSCAT surface wind retrievals. J Atmos Ocean Technol 21:1216–1231

Nagura M, McPhaden MJ (2010a) Wyrtki jet dynamics: seasonal variability. J Geophys Res 115:C07009. doi:10.1029/2009JC005922

Nagura M, McPhaden MJ (2010b) Dynamics of zonal current variations associated with the Indian Ocean dipole. J Geophys Res 115:C11026. doi:10.1029/2010JC006423

Nagura M, McPhaden MJ (2012) The dynamics of wind-driven intraseasonal variability in the equatorial Indian Ocean. J Geophys Res 115:C07009. doi:10.1029/2011JC007405

Nidheesh AG, Lengaigne M, Unnikrishnan AS, Vialard J (2012) Decadal sea level variability in the tropical Indo-Pacific—results from an ocean model and the CMIP3 databse. Clim Dyn (in revision)

Oost WA, Komen GJ, Jacobs CMJ, Van Oort C (2002) New evidence for a relation between wind stress and wave age from measurements during ASGAMAGE. Bound Layer Meteor 103:409–438

Payne RE, Huang K, Weller RA, Freitag HP, Cronin MF, McPhaden MJ, Meinig C, Kuroda Y, Ushijima N, Reynolds RM (2002) A comparison of buoy meteorological systems. WHOI Technical Report WHOI-2002-10. Woods Hole Oceanographic Institution

Pegion PJ, Bourassa MA, Legler DM, O'Brien JJ (2000) Objectively derived daily "winds" from satellite scatterometer data. Mon Weather Rev 128:3150–3168

Plueddemann AJ, Weller RA, Lukas R, Lord J, Bouchard PR, Walsh MA (2006) WHOI Hawaii ocean timeseries station (WHOTS): WJOTS-2 Mooring turnaround cruise report. WHOI. Technical Report WHOI-2006-08, Woods Hole Oceanographic Institution

Praveen Kumar B, Vialard J, Lengaigne M, Murty VSN, McPhaden MJ (2012) TropFlux: air-sea fluxes for the global tropical oceans—description and evaluation. Clim Dyn 38:1521–1543. doi:10.1007/s00382-011-1115-0

Rienecker MM, Atlas R, Schubert SD, Willett CS (1996) A comparison of surface wind products over North Pacific Ocean. J Geophys Res 101:1011–1023

Risien CM, Chelton DB (2008) A global climatology of surface wind and wind stress fields from eight years of QuikSCAT scatterometer data. J Phys Oceanogr 38:2379–2413

Rodrigues RR, Rothstein LM, Wimbush M (2007) Seasonal variability of the south equatorial current bifurcation in the Atlantic Ocean: a numerical study. J Phys Oceanogr 37:16–30

Saji NH, Goswami BN, Vinayachandran PN, Yamagata T (1999) A dipole mode in the tropical Indian Ocean. Nature 401:360–363

Satheesan K, Sarkar A, Parekh A, Kumar MR, Kuroda Y (2007) Comparison of wind data from QuikSCAT and buoys in the Indian Ocean. Int J Remote Sens 28:2375–2382

Schlax MG, Chelton DB, Freilich MH (2001) Sampling errors in wind fields constructed from single and tandem scatterometer datasets. J Atmos Ocean Technol 18:1014–1036

Schott FA, McCreary JP Jr (2001) The monsoon circulation of the Indian Ocean. Prog Oceanogr 51:1–123

Sengupta D, Senan R, Goswami BN, Vialard J (2007) Intraseasonal variability of equatorial Indian Ocean zonal currents. J Clim 20:3036–3055

Serra YL, A'Hearn P, Freitag HP, McPhaden MJ (2001) ATLAS self-siphoning rain gauge error estimates. J Atmos Ocean Technol 18:1989–2002

Smith SD (1988) Coefficients for sea surface wind stress, heat flux and wind profiles as a function ow wind-speed and temperature. J Geophys Res 93:15467–15472

Tokinaga H, Xie S-P (2011) Wave and Anemometer-based Sea-surface Wind (WASWind) for climate change analysis. J Climate 24:267–285

Vialard J, Menkes C, Boulanger J-P, Delecluse P, Guilyardi E, McPhaden MJ, Madec G (2001) Oceanic mechanisms driving the SST during the 1997–1998 El Niño. J Phys Oceanogr 31:1649–1675

Vialard J, Shenoi SSC, McCreary JP, Shankar D, Durand F, Fernando V, Shetye SR (2009) Intraseasonal response of Northern Indian Ocean coastal waveguide to the Madden-Julian Oscillation. Geophys Res Lett 36:L14605. doi:10.1029/2008GL037010

Vialard J, Jayakumar A, Gnanaseelan C, Lengaigne M, Sengupta D (2012) Processes of intraseasonal sea surface temperature variability in the Northern Indian Ocean during boreal summer. Clim Dyn 38:1901–1916

Wang C, Picaut J (2004) Understanding ENSO physics—a review. In: Wang C, Xie S-P, Carton JA (eds) Earth's climate: the ocean atmosphere interaction. AGU, Washington, pp 21–48

Webster P, Lukas R (1992) TOGA-COARE the coupled ocean-atmosphere response experiment. Bull Am Meteor Soc 73:1377–1416

Webster PJ, Moore AM, Loschnigg JP, Leben RR (1999) Coupled ocean atmosphere dynamics in the Indian Ocean during 1997–98. Nature 401:356–360

Weller RA, Baumgartner MF, Josey SA, Fischer AS, Kindle J (1998) Atmospheric forcing in the Arabian Sea during 1994–1995: observations and comparisons with climatology and models. Deep-Sea Res 45:1961–1999

Wheeler M, Hendon HH (2004) An All-Season Real-time Multivariate MJO index: development of the index for monitoring and prediction in Australia. Mon Weather Rev 132:1917–1932

Whelan SP, Weller RA, Lukas R, Bradley F, Lord J, Smith J, Bahr F, Lethaby P, Snyder J (2007) WHOTS-3 Mooring turnaround cruise report. WHOI. Technical Report, WHOI-2007-03, Woods Hole Oceanographic Institution

Wyrtki K (1973) An equatorial jet in the Indian Ocean. Science 181:262–264

Xie S-P, Carton JA (2004) Tropical Atlantic variability: patterns, mechanisms, and impacts. In: Wang C, Xie S-P, Carton JA (eds) Earth's climate: the ocean-atmosphere interaction, Geophys Monogr Ser, vol 147. AGU, Washington, pp 121–142

Yelland M, Taylor PK (1996) Wind stress measurements from the open ocean. J Phys Oceanogr 26:541–558

Yu L, Jin X, Weller RA (2007) Annual, seasonal, and interannual variability of air sea heat fluxes in the Indian Ocean. J Clim 20:3190–3209

Zhang C (2005) Madden-Julian oscillation. Rev Geophys 43:RG2003. doi:10.1029/2004RG000158

Zhang X, McPhaden MJ (2006) Wind stress variations and interannual sea surface temperature anomalies in the eastern equatorial Pacific. J Clim 19:226–241